2014-01-01

# An Experimental Investigation on Liquid Methane Convection and Boiling in Rocket Engine Cooling Channels

Abraham Trujillo
*University of Texas at El Paso*, agtrujillo@miners.utep.edu

# AN EXPERIMENTAL INVESTIGATION OF LIQUID METHANE CONVECTION AND BOILING IN ROCKET ENGINE COOLING CHANNELS

ABRAHAM GERARDO TRUJILLO

Department of Mechanical Engineering, ME

APPROVED:

Ahsan Choudhuri, Ph.D., Chair

Norman Love, Ph.D.

Cristian Botez, Ph.D.

Bess Sirmon-Taylor, Ph.D.
Interim Dean of the Graduate School

# Dedication

This work is dedicated to my family and friends who have supported me throughout my entire education.

# AN EXPERIMENTAL INVESTIGATION OF LIQUID METHANE CONVECTION AND BOILING IN ROCKET ENGINE COOLING CHANNELS

by

ABRAHAM GERARDO TRUJILLO, B.S. Mechanical Engineering

THESIS

Presented to the Faculty of the Graduate School of

The University of Texas at El Paso

in Partial Fulfillment

of the Requirements

for the Degree of

MASTER OF SCIENCE

Department of Mechanical Engineering

THE UNIVERSITY OF TEXAS AT EL PASO

August 2014

## Acknowledgements

I would like to thank NASA Johnson Space Center (JSC) for the financial support to enable the completion of this project. The material in this project is based upon work supported by NASA under award No(s) NNX09AV09A. I would also like to express my gratitude to my supervisor, Dr. Ahsan Choudhuri from the University of Texas at El Paso and my mentor Dr. John C. Melcher from NASA JSC, whose guidance and experience have been very important in the completion of this work.

# Abstract

In the past decades, interest in developing hydrocarbon-fueled rocket engines for deep spaceflight missions has continued to grow. In particular, liquid methane ($LCH_4$) has been of interest due to the weight efficiency, storage, and handling advantages it offers over several currently used propellants. Deep space exploration requires reusable, long life rocket engines. Due to the high temperatures reached during combustion, the life of an engine is significantly impacted by the cooling system's efficiency. Regenerative (regen) cooling is presented as a viable alternative to common cooling methods such as film and dump cooling since it provides improved engine efficiency. Due to limited availability of experimental sub-critical liquid methane cooling data for regen engine design, there has been an interest in studying the heat transfer characteristics of the propellant. For this reason, recent experimental studies at the Center for Space Exploration Technology Research (cSETR) at the University of Texas at El Paso (UTEP) have focused on investigating the heat transfer characteristics of sub-critical $CH_4$ flowing through sub-scale cooling channels. To conduct the experiments, the csETR developed a High Heat Flux Test Facility (HHFTF) where all the channels are heated using a conduction-based thermal concentrator. In this study, two smooth channels with cross sectional geometries of 1.8 mm x 4.1 mm and 3.2 mm x 3.2 mm were tested. In addition, three roughened channels all with a 3.2 mm x 3.2 mm square cross section were also tested. For the rectangular smooth channel, Reynolds numbers ranged between 68,000 and 131,000, while the Nusselt numbers were between 40 and 325. For the rough channels, Reynolds numbers ranged from 82,000 to 131,000, and Nusselt numbers were between 65 and 810. Sub-cooled film-boiling phenomena were confirmed for all the channels presented in this work. Film-boiling onset at Critical Heat Flux (CHF) was correlated to a Boiling Number (Bo) of approximately 0.1 for all channels. Convective Nusselt number follows predicted trends for Reynolds number with a wall temperature correction for both the boiling and non-boiling regimes.

# Table of Contents

# List of Tables

# List of Figures

# Chapter 1: Introduction

## 1.1 Project Overview

The interest in developing reusable, long-life rocket engines has continued to grow in recent years. Liquid Oxygen (LOX)-Hydrocarbon liquid rocket engines are seen as attractive candidates for high performance and reusable applications because they offer high propellant bulk density and relatively high performance [1]. A particular hydrocarbon of interest is liquid methane ($LCH_4$). $LCH_4$ is seen as a good candidate due to the weight efficiency, storage, and handling advantages it offers over several currently used rocket engine propellants. For instance, $LCH_4$ temperatures are similar to that of LOX, eliminating the need for separate storage equipment and technology. Additionally, $LCH_4$ is approximately five times denser than hydrogen ($H_2$) which can reduce the payload and the overall cost while increasing the performance for long duration space missions. Furthermore, $LCH_4$ is non-toxic unlike hypergolic propellants such as monomethylhydrazine (MMH) and nitrogen tetraoxide (NTO) which create complications regarding storage and handling. Also, another advantage of $LCH_4$ is its potential application in In Situ Resource Utilization (ISRU) [2]. However, such previously mentioned applications lead to high temperatures during combustion, and therefore an effective cooling system is necessary to prevent engine failure. Regeneratively-cooled (regen) engine design is seen as a viable alternative because of the advantages regenerative cooling presents in comparison to dump cooling or film cooling; more specifically, regen engines offer improved cooling and higher engine efficiency, translating into extended spaceflight durations. The method of regenerative cooling consists in using the actual rocket fuel as the coolant by flowing it through the outer walls of the rocket nozzle and combustion chamber via cooling channels before being combusted. Figure 1.1 shows the only subcritical LOX/Methane regen engine that has been fired until now.

Figure 1.1: XCOR XR-5M15 LOX/Methane Regen Subcritical Pressure-Fed Engine [3]

Currently, NASA Johnson Space Center (JSC) is developing a vehicle that integrates new green propulsion, guidance, navigation and control systems, and autonomous landing and hazard detection technology known as Project Morpheus [4]. Morpheus integrates lander class engines that function with a LOX/Methane propulsion system. Typical lander class engines operate using a blow-down system where the pressures are subcritical. Moreover, NASA aims to develop a regen LOX/Methane rocket engine for Morpheus. However, one of the challenges with subcritical methane regen engine design is that there is limited empirical data regarding subcritical methane heat transfer. To provide empirical subcritical $LCH_4$ cooling data, the High Heat Flux Test Facility (HHFTF) was developed at the center for Space Exploration Technology Research (cSETR) at the University of Texas at El Paso (UTEP) focusing on the study of sub-scaled single cooling copper channels.

## 1.2 Project Objectives

The purpose of this study is to experimentally investigate the heat transfer characteristics of subcritical methane using sub-scale single cooling channels at steady state conditions, i.e. heat flux, bulk properties, and channel wall temperatures. More specifically, the project is divided into two main objectives. The first objective is to further the boiling analysis of a smooth rectangular channel. The

following objective of this experimental investigation is to study the effects of surface roughness on cooling channels subjected to conditions similar to those encountered in lander class engines. For that reason, three channels with different roughness finishes will be compared to a smooth channel. The cross-sectional geometry will be kept the same for all channels. By keeping the channel cross-sectional geometry constant and increasing the surface roughness it is expected that the cooling effectiveness will increase at the penalty of increased pressure drops. The surface finishes selected are typical of milled channels. Common surface finishes produced by milling range from 0.80 to 6.3 microns (μm) based on the arithmetic mean value roughness scale ($R_a$) [5].

### 1.3 Experimental Approach

In an attempt to fundamentally understand the heat transfer behavior of propellants, several heat flux facilities (HHF) have been developed. Typically, these facilities are designed to provide a constant heat flux to a test specimen. HHFs incorporate heating techniques such as arc heating, resistive heating, and conduction heating, being the latter two the most commonly used techniques for rocket engine applications. In this study, all test section cooling channels will be heated using a conduction-based thermal concentrator due to the advantages conduction heating offers over resistive heating; that is, a conduction heat flux facility provides asymmetric heating which better simulates the heat encountered in a rocket engine due to combustion. To supply the cSETR's HHFTF with liquid methane, a 13 L condenser has been developed at the cSETR. The condenser is capable of providing sufficient LCH4 to reach steady state conditions under the already discussed lander class parameters.

### 1.4 Relevance

The results from this experiment will attempt to give a better understanding of the heat transfer characteristics of subcritical $LCH_4$. This data is relevant to designers attempting to either verify or build around a design case using the parameters met in this study. This study will also provide a means of verification for CFD simulations performed by researchers in test cases pertaining to this study. In conjunction, the effects of surface roughness and boiling on subcritical methane will be studied. All of the above statements are important contributing factors in the analysis for a final product especially in the aerospace industry.

# Chapter 2: Literature Review

## 2.1 High Heat Flux Facilities

Subscale HHFs facilities applying turbulent internal forced convection through a heated tube have been developed to investigate the heat transfer characteristics of liquid propellants applicable to regen engines. Subscale HHFs incorporate heating techniques such as arc heating, resistive heating, and conduction heating facilities have been utilized to study and ultimately predict the cooling performance of coolants at various testing conditions. The subscale test facilities using conductively heated tubes and resistively heated tubes were the most relevant to this study and are therefore presented.

### 2.1.1 Conductively Heated Tube Facilities

In conduction based heat flux facilities the main source of heat is a heating block that is put into direct contact with a test section channel. The main advantage is that conduction facilities offer the closest simulation to what happens during combustion in a rocket chamber as opposed to resistively heated facilities; that is, they have the ability to asymmetrically heat test sections to represent the hot-wall and cold-wall sides of a regeneratively-cooled rocket engine cooling jacket, where the heat from the copper block resembles the heat generated by the combustion of propellants inside the combustion chamber. In addition, the electrically driven chemical phenomena that usually leads to potential degradation of the tube materials that is seen in resistively heated facilities is not seen in conductively heated facilities. Aerojet TechSystems and the AFRL have previously used conduction based facilities [6].

**Aerojet**

Aerojet TechSystems performed the Hydrocarbon-Fuel/Combustion-Chamber-Liner Materials Compatibility Program for NASA Lewis Research Center in the late 1980s with several major objectives which basically aimed to define the corrosive interaction process that occurs between hydrocarbon fuels and combustion chamber liner materials; and consequently, develop and evaluate protective measures to remedy the defined corrosive interaction process. This research was motivated by the studies conducted by the United Technologies Research Center and Rockwell International Rocketdyne Division where severe copper corrosion and carbon deposition were found using resistively heated tubes.

The Aerojet Carbothermal Materials Tester used a large copper block heated by ten electrically insulated cartridge heaters embedded in the block. Moreover, the heat produced by the heaters is transferred by conduction onto a test section made of copper. The test sections incorporated a 0.5-mm square cooling channel milled at the bottom. The rig allowed for geometrically concentrating energy and transferring it onto a test specimen. The configuration of the Aerojet Carbothermal Rig is shown in Figure 2.1. When tested with methane, the Aerojet Carbothermal Rig reached a maximum heat flux of 85.0 $MW/m^2$, wall temperatures ranging from 343 to 499°C, and pressured up to 28.9 MPa [7].

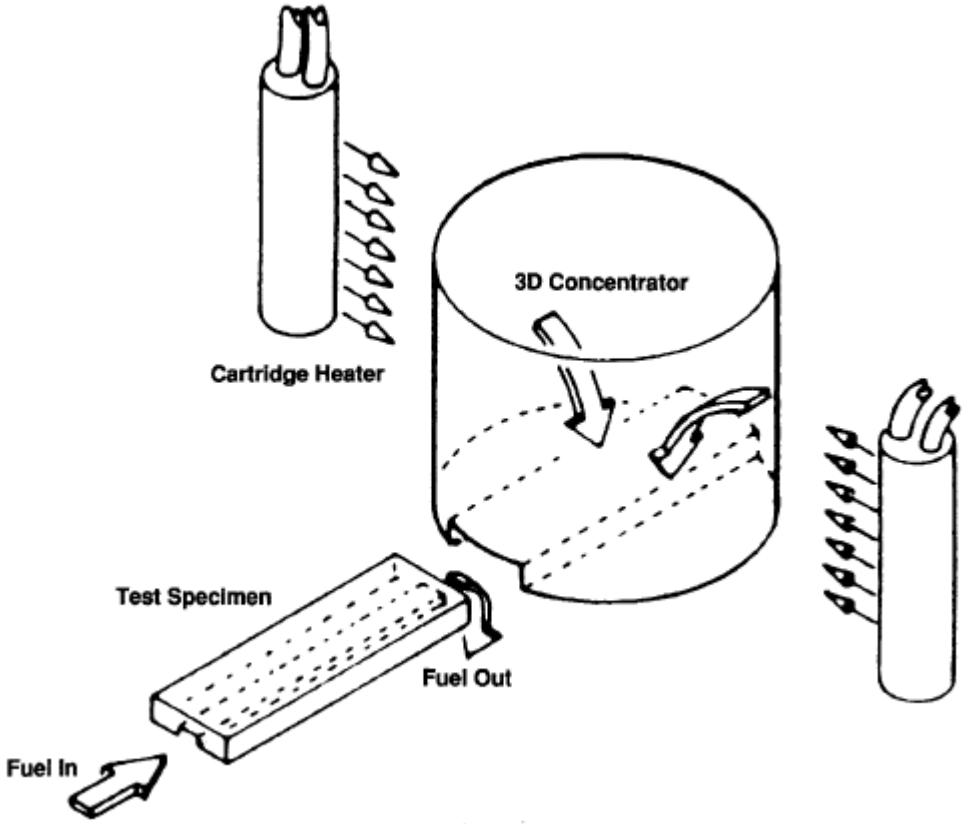


Figure 2.1: Aerojet Carbothermal Rig Configuration [7]

**Air Force Research Laboratory**

With the interest in developing reusable hydrocarbon-fueled engine technologies for reusable launch vehicles, the Air Force Research Laboratory (AFRL) conducted a series of studies from 2004 to

2008 with the goal of understanding the thermal stability of hydrocarbon fuels under high heat fluxes encountered in regenerative cooling. To meet the high reliability and reusability requirements proposed for the above mentioned engines, the AFRL developed a High Heat Flux Facility (HHFF) as an extension of the Aerojet Carbothermal Rig. In specific, the HHFF was developed to experimentally investigate the cross sectional geometry effects on RP-2 fuel using copper channels. In 2004, simulations were run to select an optimal heating block configuration and a first generation rig was constructed. The 1st generation HHFF rig consisted of a heating block with embedded heating cartridges which then conductively heated a copper test section channel. The tapered section of the block allows for the heat to be geometrically focused. A key main feature of the rig was the ability to change the geometry of the channel by just swapping test sections. In addition, the system was placed in a vacuum chamber to simulate an environment similar to altitude conditions and to also prevent oxidation on the block and test sections. This system was capable of achieving heat fluxes up to 163.5 MW/m$^2$ and operating at pressures up to 31.0 MPa [6, 8]. Figure 2.2 shows the configuration of the AFRL's HHFF.

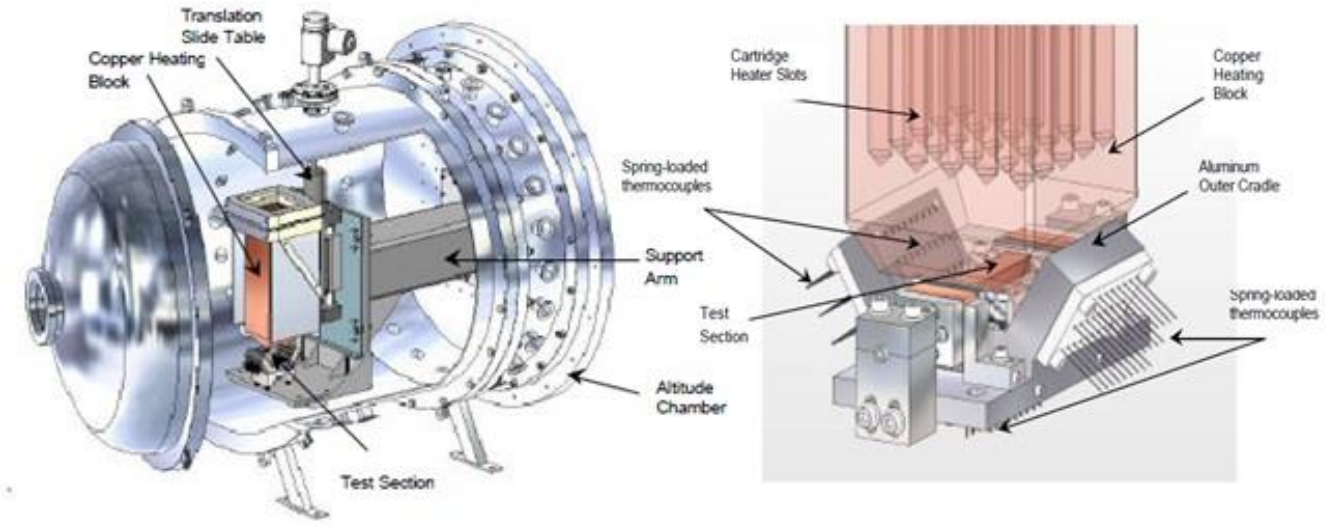


Figure 2.2: AFRL High Heat Flux Facility [9]

However, the original setup resulted in poor heat transfer due to contact resistance, misalignment, and conductive losses. For that reason, an improved configuration was built. Instead of having the test section separate from the block, the upper holder component of the test section was

removed and the cooling channel was integrated by machining the channel geometry into the block. Figure 2.3 (a) shows the configuration of the heating block-test section presented in 2004, and a modified configuration is shown in Figure 2.3 (b) [10]. The main disadvantage of this configuration was that a new block had to be machined for each channel [10].

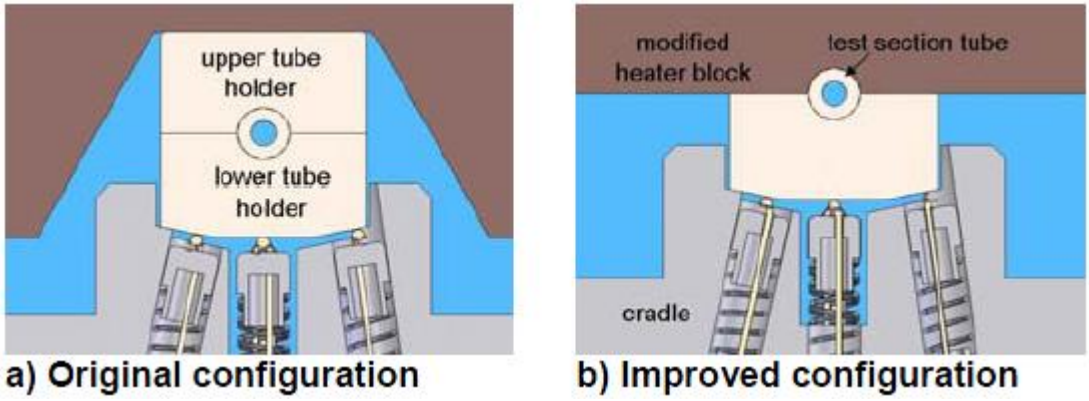


Figure 2.3: (a) AFRL HHFF Original Configuration. (b) AFRL HHFF Improved Configuration [10]

### 2.1.2 Resistively Heated Tube Facilities

Resistively heated tube facilities, also known as electrically heated tube facilities, use a method of heating known as direct ohmic heating which consists in passing a current through a tube in order to reach high wall temperatures. In contrast to conductively heated tube facilities where the heat transfer to the fuel is asymmetric, the heat transfer to the fuel in electrically heated tubes is circumferential. Some of the main drawbacks for resistively heated tube facilities are that power requirements can be extreme for copper tubes [6]. Rocketdyne and NASA Glen Research Center (GRC) have used resistively heated tubes to study the cooling characteristics of $LCH_4$.

**Rocketdyne/NASA MSFC**

Rocketdyne conducted a 12-month program for NASA Marshall Space Flight Center (MSFC). Testing was conducted at the Rockwell North American Aviation Operations (NAAO) Aerothermal Laboratory. The program was an experimental investigation with the purpose of determining the coking thresholds and cooling properties of methane and liquid natural gas (LNG) on copper test specimens [1]. With the motivation of developing reusable, high-performance, liquid rocket booster engines that require

copper-base alloy cooling channels similar to the Space Shuttle Main Engine (SSME) the Rocketdyne rig was designed to simulate the pressure and heat flux operating conditions of the Main Combustion Chamber (MCC). The electrical power was provided by three AC reactors rated at 2000 amps. In addition, the system incorporated a methane run tank with a capacity of 132.5 liters (L). The test specimens were bimetallic tubes with an inside diameter of 1.9 mm and with lengths of 76.2 and 177.8 mm. The rig was capable of reaching heat fluxes up to 139.0 MW/m$^2$, wall temperatures between 316 and 482°C, and working pressures up to 31.0 MPa [1]. Rocketdyne's experimental setup is shown Figure 2.4.

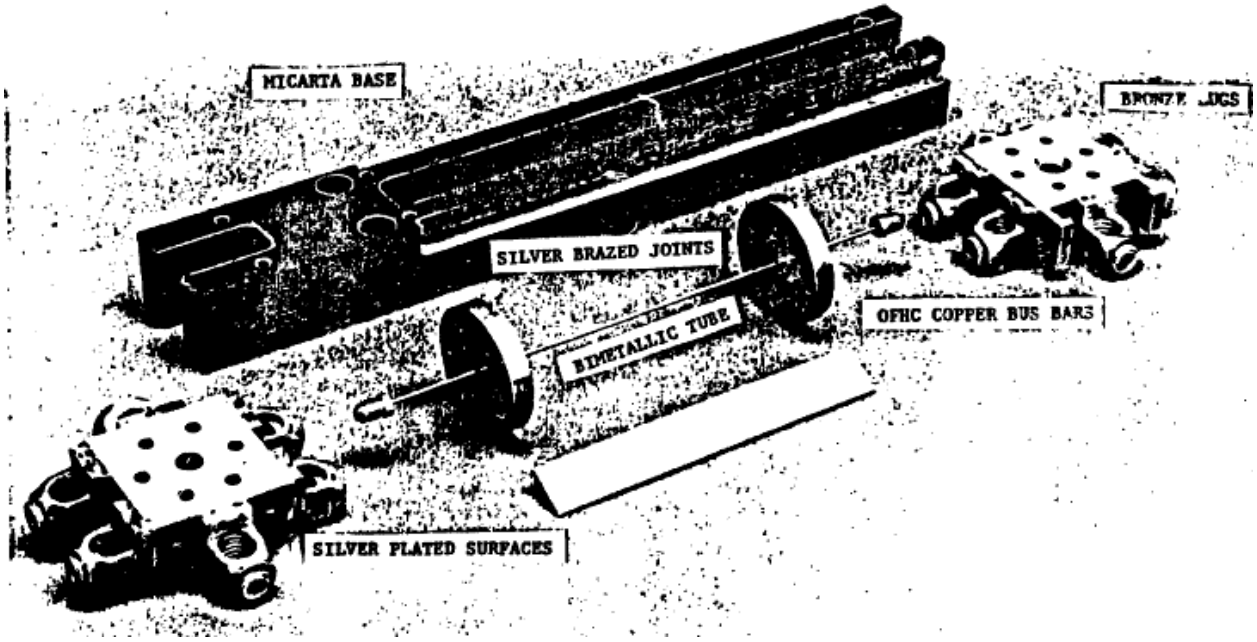


Figure 2.4: Rocketdyne-MSFC Components for the Resistively Heated HHF [1]

**NASA Glen Research Center**

In 2010, an experimental investigation on the heat transfer characteristics of liquid and two-phase methane was conducted at the NASA Glen Research Center Heated Tube Facility (HTF) using resistively heated tubes [11]. The rig incorporated test sections that were heated using a 1500 A, 100 VDC power supply. Four test sections were machined using Inconel 600 tubes with diameters varying from 2.1 mm for two of the test sections, and 1.4 mm and 0.7 mm for the remaining ones. All the test sections had a wall thickness of 0.5 mm and had a length of 368.3 mm. For wall temperature measurement, a total of fifteen thermocouples were spot welded along every test section. The HTF was

able to reach heat fluxes up to 10.1 MW/m$^2$ and wall temperatures up to 1000 K [11]. The GRC HTF is shown in Figure 2.5.

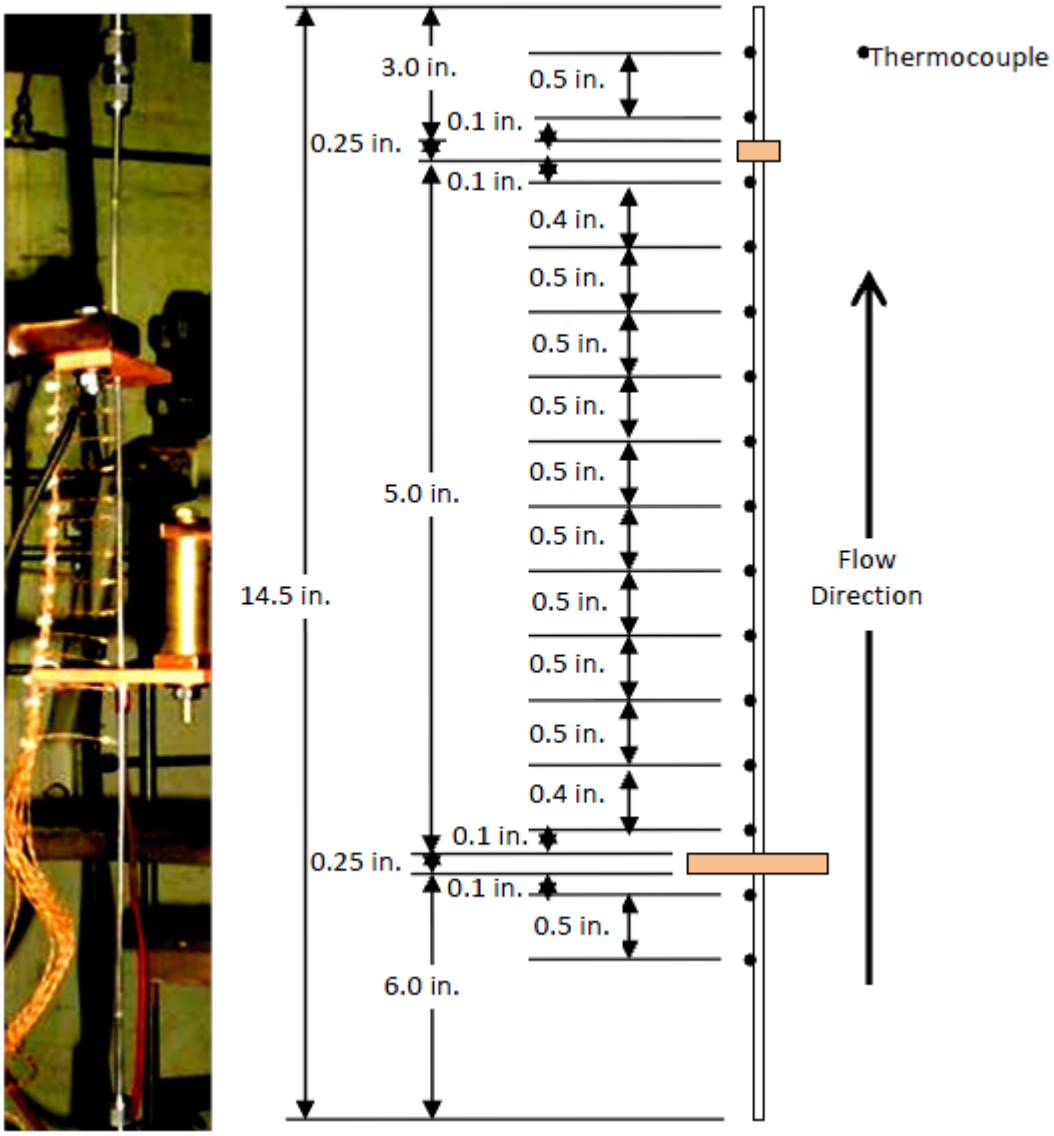


Figure 2.5: NASA GRC Heated Tube Facility [11]

## 2.2 Liquid Methane Heat Transfer Studies

The growing interest in liquid methane as a potential rocket propellant as well as the lack of liquid methane heat transfer data have led to the experimental investigation of the heat transfer characteristics of methane. As previously mentioned, $LCH_4$ is seen as a viable alternative due to the weight efficiency, storage, handling, and relatively high performance advantages it offers over several

currently used rocket engine propellants such as hydrogen and hypergolic propellants; in addition, the potential application in ISRU is another advantage of $LCH_4$. However, the cooling capabilities of $LCH_4$ have not been fully described in contrast to other propellants. Several studies have been conducted to characterize the cooling properties of methane at both subcritical and supercritical conditions.

### 2.2.1 Rocketdyne-NASA MSFC

The previously mentioned Rocketdyne and NASA MSFC collaboration program reported by Cook aimed to study the heat transfer characteristics of both liquid natural gas (LNG) and $LCH_4$ through resistively heated copper smooth and roughened bimetallic tubes and to determine the coking thresholds of the copper channels [1]. The heat transfer data provided by Rocketdyne was reported at similar operating conditions such as mass flux, heat flux, wall temperature, and fluid pressure of the MCC based on the design of the SSME. For the LNG tests, the Nusselt number ranged from 1067 to 5844, the Reynolds number ranged from 8.2 E5 to 3.8 E6, and the heat flux was varied from 2.6 to 139.0 $MW/m^2$. Moreover, convective correlations to predict the Nusselt number were developed for both smooth and roughened tubes. Also, a corrosive reaction between copper and methane was demonstrated while no significant coking was detected [1]. Figure 2.6 and Figure 2.7 show Rocketdyne's methane Nusselt number correlations for smooth and rough tubes, respectively.

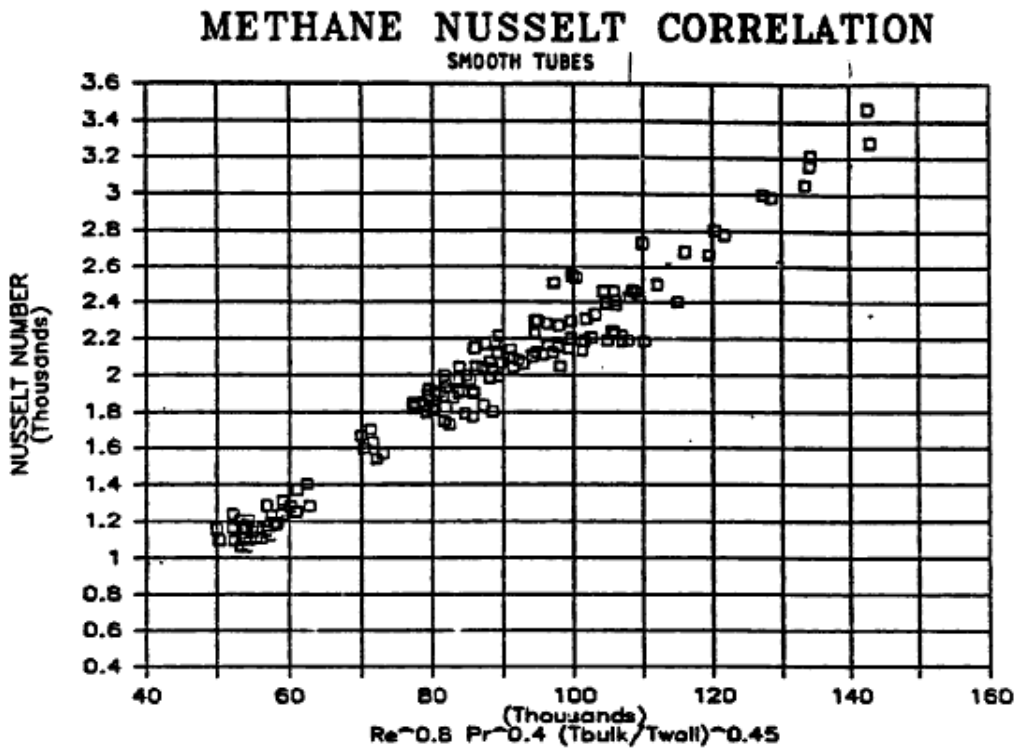


Figure 2.6: Rocketdyne Methane Nusselt Correlation for Smooth Tubes [1]

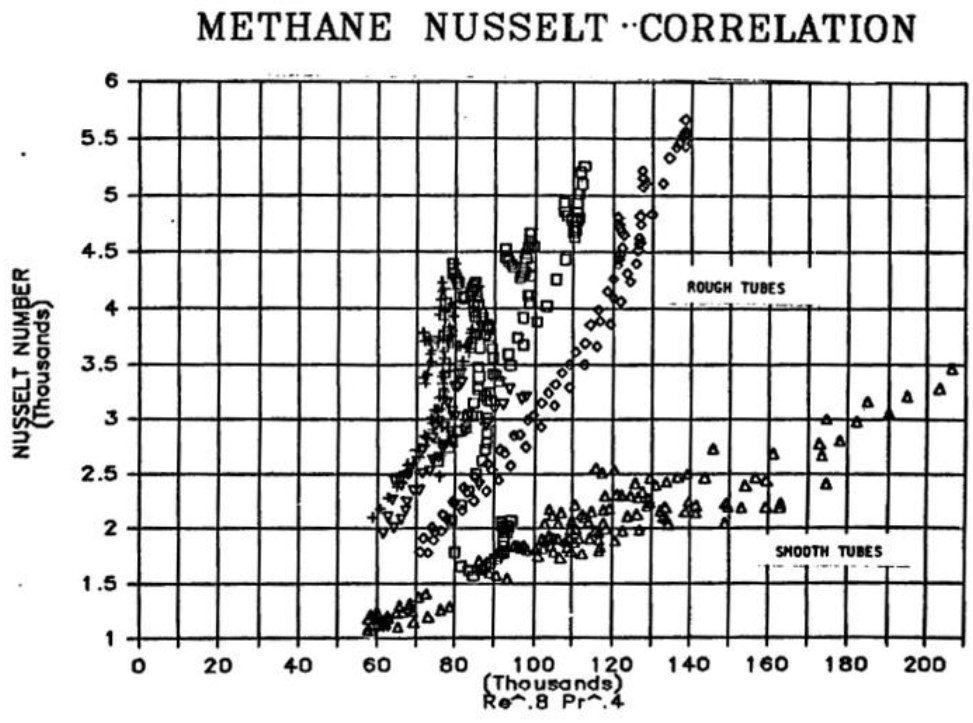


Figure 2.7: Rocketdyne Methane Nusselt Correlation for Rough Tubes [1]

### 2.2.2 NASA Glen Research Center

An experimental investigation on the heat transfer of liquid and two-phase methane was conducted by Van Noord at the NASA Glen Research Center Heated Tube Facility (HTF) using resistively heated Inconel 600 tubes in 2010 [11]. The primary objective for the experiment was to produce heat transfer correlations for methane in the liquid and two-phase regime below critical pressures and appropriate to pressure-fed engines. The experiment obtained fifty six data points with flow velocities from 2.47 to 47.9 m/s, outlet pressures ranging from 1.5 to 3.9 MPa, inlet pressures ranging from 1.6 to 5.5 MPa, methane subcooling from 104 to 142 K, and average heat fluxes up to 10.1 $MW/m^2$. For two-phase flow testing, critical heat flux values were determined where nucleate boiling transitions to film boiling and were plotted as a function of Velocity and Wall Temperature as shown in Figure 2.8. The change from nucleate to film boiling was quite pronounced for test section pressures less than 2.1 MPa. On the other hand, the change from nucleate to film boiling was more subtle at pressures above 3.1 MPa. A secondary goal of the testing was to measure system pressure drops in the two-phase regime [11].

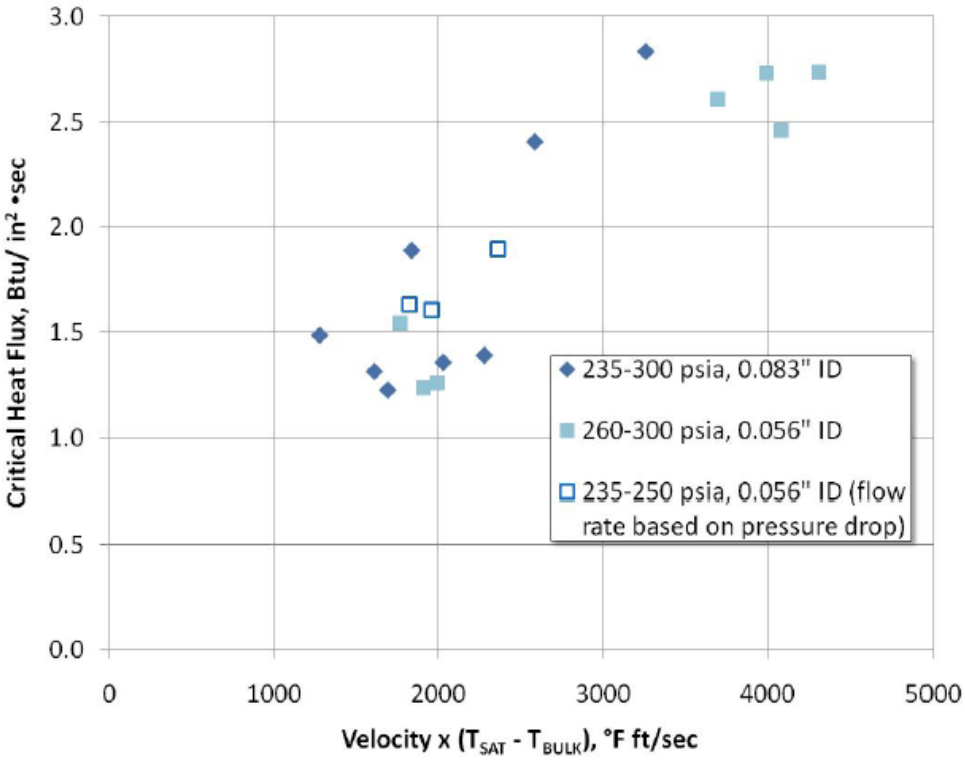


Figure 2.8: Van Noord's methane critical heat flux data for a range pressures [11]

### 2.2.3 Pratt and Witney Aircraft Division

Glickstein and Whitesides performed a study to evaluate the heat transfer behavior of several aliphatic hydrocarbons, including methane, in nucleate and film boiling using resistively heated Inconel 600 tubes. The experiment was conducted at the Pratt and Whitney Aircraft Corporation of the United Aircraft Corporation in 1967. One of the main goals was to determine the effects of the fluid state and mass velocity on maximum nucleate boiling heat flux and film boiling heat-transfer coefficients [12]. Data was reported at both subcritical and supercritical conditions. An equation for heat flux was developed that correlated with all the maximum nucleate-boiling data for each fluid as shown in Figure 2.9. In addition, a single convective correlation for several hydrocarbons, among them methane, was developed at the saturated film-boiling state. Moreover, convective correlations were also derived for subcritical film boiling and supercritical forced convection data for each fluid [12].

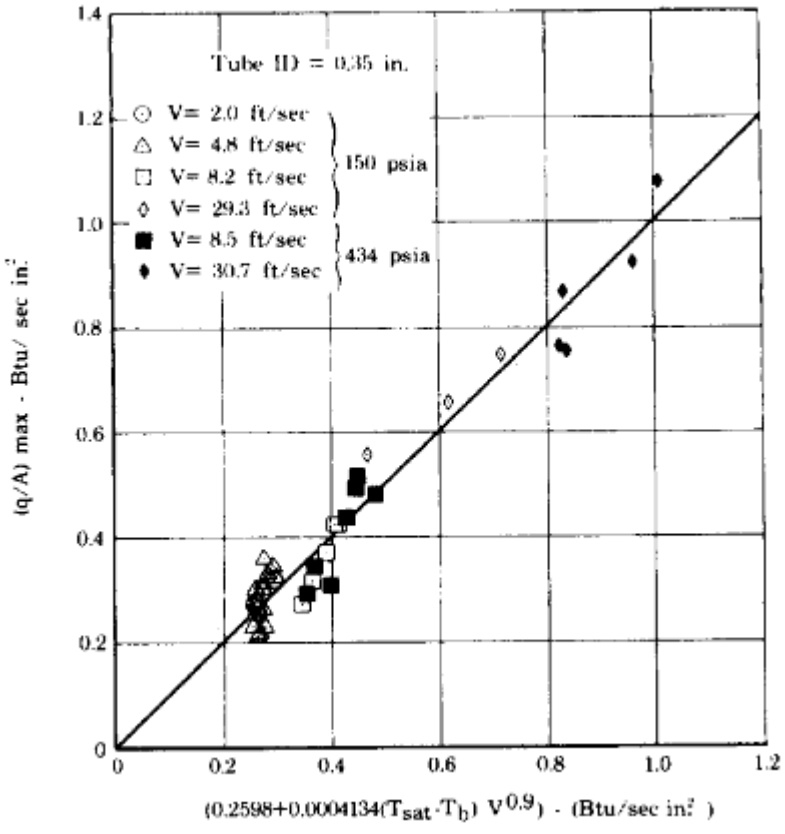


Figure 2.9: Correlation of maximum nucleate boiling heat flux data for methane by Glickstein and Whitesides [12]

### 2.2.4 Xi'an Jiaotong University

In 2013, Hongfang performed an experimental investigation at the State Key Laboratory of Multiphase Flow in Power Engineering at the Xi'an Jiaotong University on the heat transfer of supercritical cryogenic methane using miniature resistively heated stainless steel tubes [13]. The test sections had a diameter of 2.6 mm and a wall thickness of 0.5 mm. The main goal of this study, was to analyze the mass flux, heat flux and pressure effects of methane near the pseudo-critical temperature, which is defined as the temperature, for a given pressure, at which the specific heat exhibits a maximum; however, due to the radical physical property variations in the vicinity of the pseudo-critical temperature, the heat transfer behavior is quite different to that of a constant property fluid [13]. The working pressures in the system ranged from 1-15 MPa, and the heat fluxes fluctuated from 1-16 MW $m^{-2}$. This experiment demonstrated that single phase correlations such as Dittus-Boelter and Gnielinski do not work well in the pseudo-critical region due to the property variations. For that reason, a semi-empirical new correlation evaluated by Probability Density Function (PDF) based time-averaged properties shown in Figure 2.10 was developed and it was able to capture more than 85% of the experimental data with a 25% error [13].

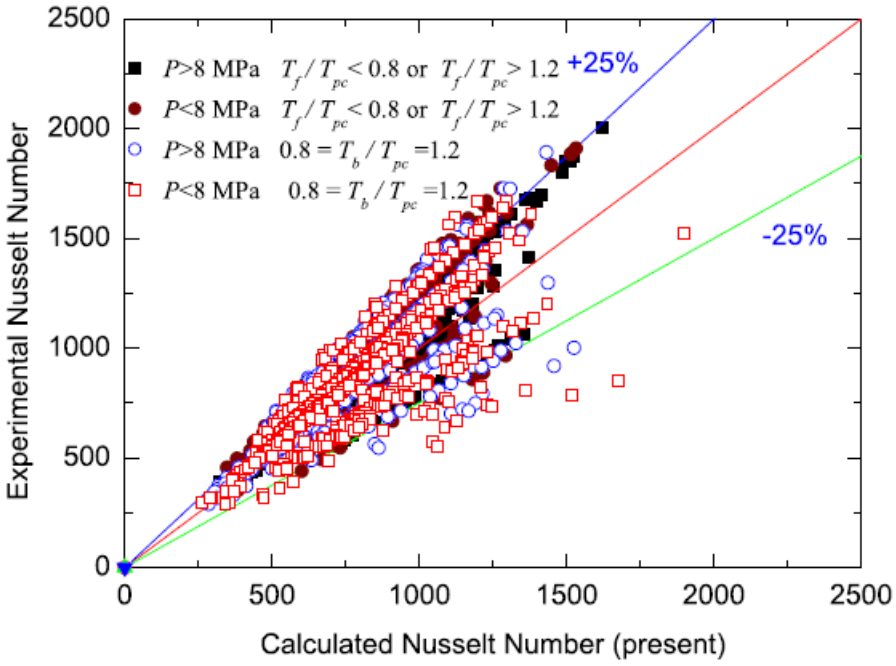


Figure 2.10: Van Noord's methane critical heat flux data for a range pressures [13]

### 2.2.5 UTEP cSETR

Two recent studies were conducted at the University of Texas at El Paso's (UTEP) center for Space Exploration Technology Research (cSETR) between 2013 and 2014 using the same HHFTF described in this study. In 2013, a copper channel with a 1.7 x 1.7 mm square cross-section machined at White Sands Test Facility (WSTF) was used to study the transient and steady state heat transfer behavior of subcritical cryogenic methane. Experimental Nusselt number data ranged from 30 to 260 while Reynolds numbers ranged from 19,000 to 140,000 as shown in Figure 2.11 [14].

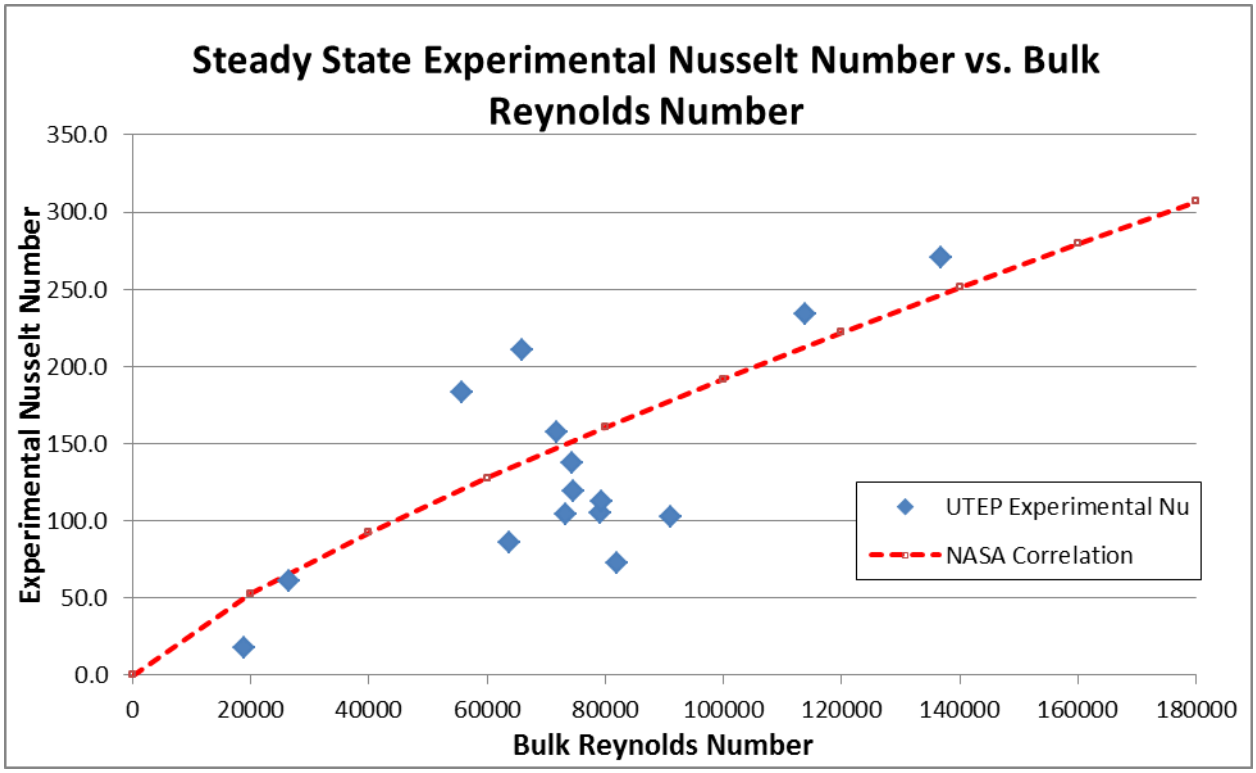


Figure 2.11: UTEP's 1.7 mm x 1.7 mm Square Channel Experimental Nusselt Number data as a Function of Bulk Reynolds Number [14]

In 2014, the cooling channel geometry effects were investigated using square, rectangular, and circular channels with dimensions of 1.8 mm x 1.8 mm, 1.8 mm x 4.1 mm and 1.8 mm x 14.2 mm considered to be a high aspect ratio cooling channel (HARCC), and inside diameters 3.2 mm and 6.32 mm, respectively [15]. Results show that each test section configuration required distinct Nu number predictions to accurately represent the empirical data. Thus, several convective correlations were used to

correlate the experimental data including the NASA-Rocketdyne [1], Jackson correlation [13], and the Klimenko correlation [16]. The circular cooling channel with an inside diameter of 3.18 mm was the best correlated channel in this study and the Klimenko correlation was employed supporting the theory of transition boiling in the channel as shown in Figure 2.12 [15].

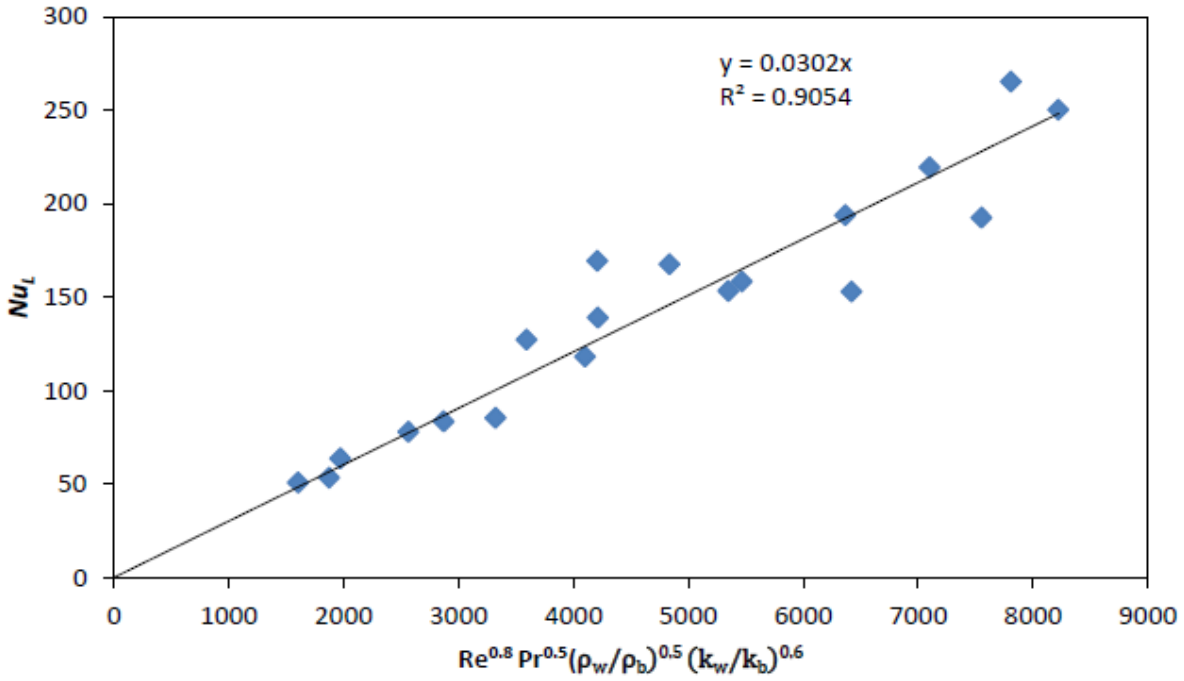


Figure 2.12: UTEP's 3.2 mm ID Channel Nusselt Number Correlation [15]

## 2.3 Heat Transfer Enhancements

Heat transfer enhancements, also known as heat transfer augmentation techniques, have been used in different industries, including the aerospace industry, to improve the heat transfer rate in heat exchanger applications. In cooling channels, heat transfer enhancements that have been used include artificial roughness, twisted tapes, wire coils, and transverse and longitudinal fins.

The previously discussed work by Cook [1], reported data were roughened cooling channels were compared to smooth cooling channels; It was shown that high tube wall roughness produced large increases in pressure drop and heat transfer.

In the study that exists in reference [17] comparisons were made between twisted tape and wire coils in tubes. It was demonstrated that twisted tape performs better than any other insert while in

turbulent flow twisted tape is not very effective because it blocks the flow and the pressure drop is large. On the other hand, wire coil performs better in turbulent flow than in laminar flow [17]. Furthermore, fins and ribs are enhancements that are generally more efficient in turbulent flow. Figure 2.13 shows an example of how twisted tapes are used in tubes.

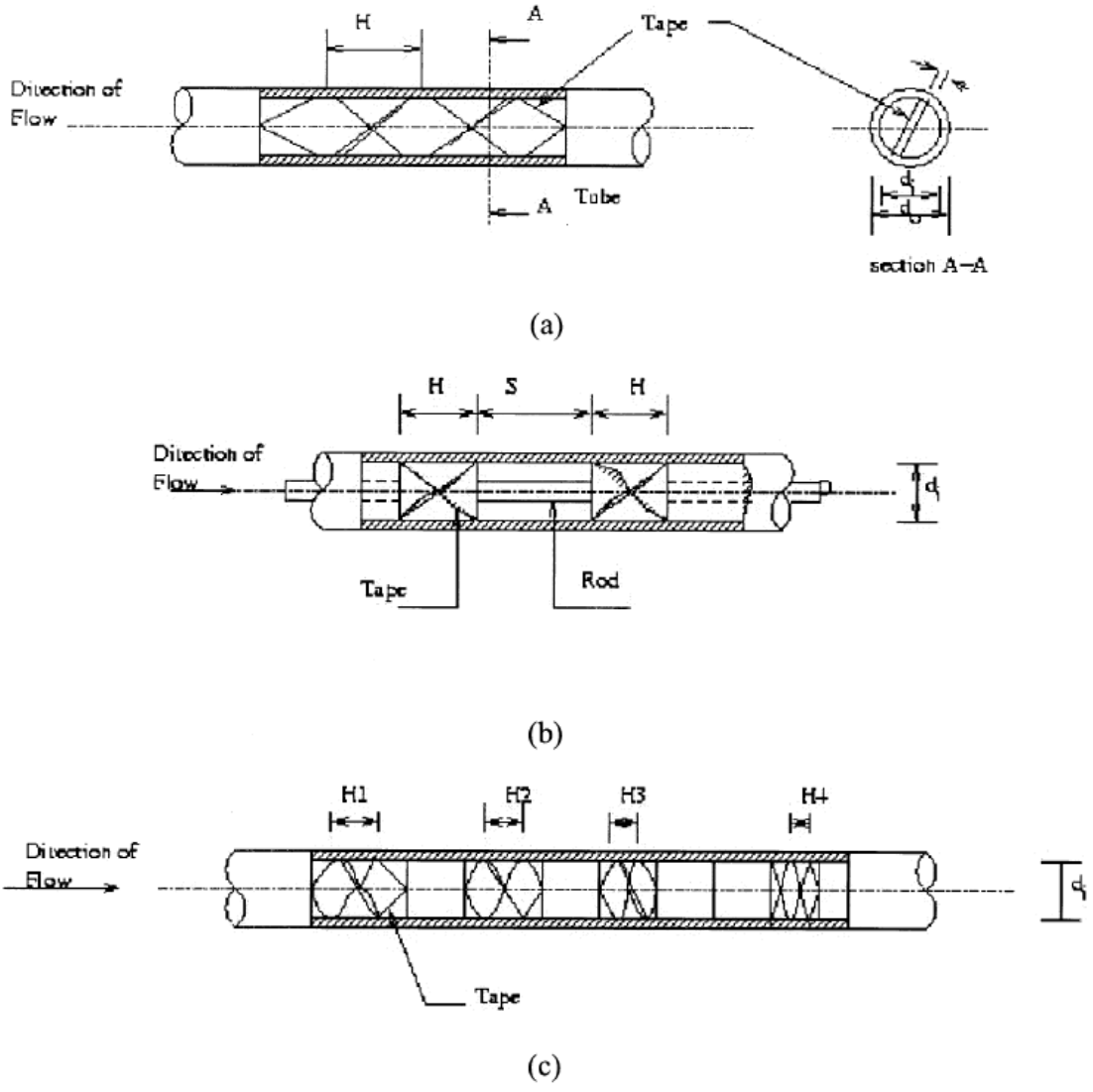


Figure 2.13: Several types of twisted tapes used in tubes to improve heat transfer [17]

# Chapter 3: High Heat Flux Test Facility

## 3.1 Design Approach

The HHFTF has been developed to study the heat transfer characteristics of subcritical $LCH_4$. The main purpose of the HHFTF is to supply a constant heat flux to test section cooling channels. The HFFTF concept is an adaptation of the Air Force Research Laboratory (AFRL) High Heat Flux Facility, described in References [6, 8, 9 and 10]. The selection of the materials for the construction of the components was based on several factors. That is, compatibility with $LCH_4$, the ability to operate when subjected to temperatures between -200 and 650°C, and operability under pressures up to 2.1 MPa. The main components of the HHFTF are a heating block, test section cooling channels, a test stand, and a cradle which are placed inside a vacuum chamber. The purpose of the vacuum chamber is to simulate altitude conditions, reduce heat losses due to convection, and to also reduce oxidation that may occur when heating the components. The function of each component is detailed next.

## 3.2 HHFTF Components

### 3.2.1 Heating Block

A block made of C12200 copper is used as the conduction-based thermal concentrator. The design of the heating block was based on the work reported by the AFRL [6, 8, 9 and 10]. The dimensions of the heating block are 10.2 cm x 10.2 cm x 17.8 cm with a 45°-angle tapered section at the top designed to geometrically focus thermal energy onto a 2.5 cm x 5.1 cm surface as illustrated in Figure 3.1. Copper was chosen as the block's material because it offers a thermal conductivity of 365.0 W/m-K and a working temperature of 760°C. In addition, 3.18 mm holes were machined at the bottom face of the block and distributed symmetrically where up to 25 heating cartridges can be inserted. The heating cartridges function as the block's heat source.

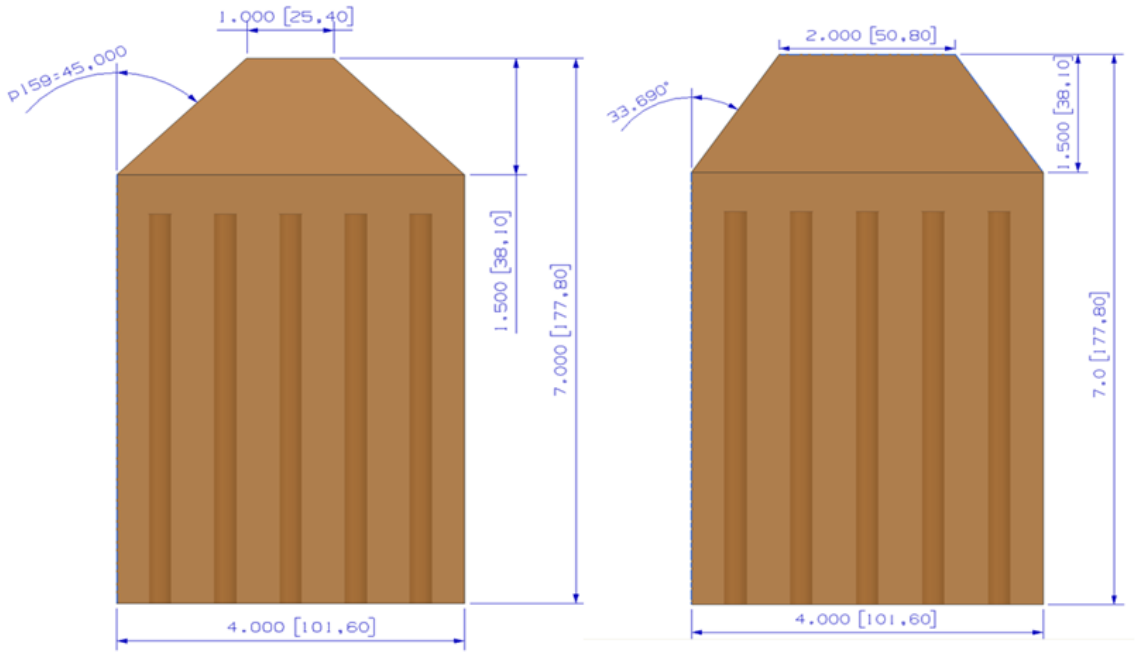


Figure 3.1: Copper Heating Block Dimensions

The heating block's radiative losses were a major concern especially at relatively high temperatures (400°C). For that reason, a preliminary experiment was conducted to investigate the heat transfer losses due to radiation by taking radiometry data as the block was heated. At the maximum testing temperature, a 2.5% radiation loss was measured. Nevertheless, the heating block is insulated with ceramic insulation that is fitted in between the cradle and the tapered section of the heating block. Additionally, the sides of the heating block are wrapped with cloth fiber insulation to minimize radiation losses from the larger surface areas; to hold the cloth fiber in place a layer of aluminum is placed around the cloth fiber as depicted in Figure 3.2.

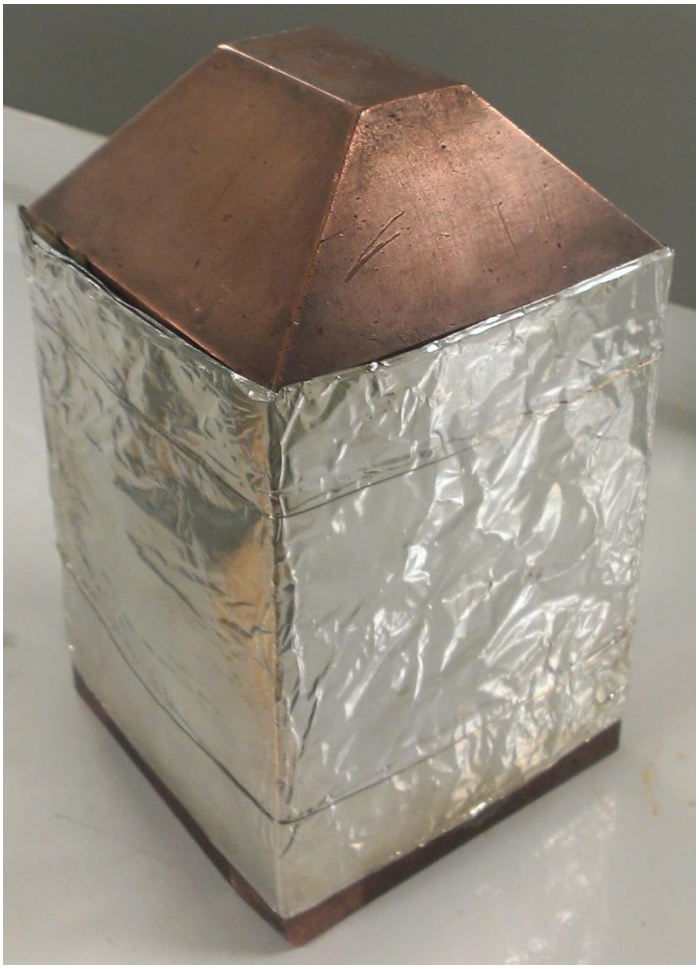

Figure 3.2: Insulated Copper Heating Block

### 3.2.2 Test Stand

The rest of the components of the HHFTF are supported by a stainless steel 316 L test stand shown in Figure 3.3. The stand holds the heating block in place using small plates that were welded onto L-shaped brackets. The plates support the corners of the block without obstructing any cartridge heater ports. Furthermore, a 5.0 cm x 5.0 cm section of the stand base was removed to allow the cartridge heater wiring to be directed underneath the test stand towards the chamber feed-through. At the top of the stand, two bolts are used to join the stand to the cradle. The stand is able to support the load created by the HHFTF system which approximately weights 17.2 kg.

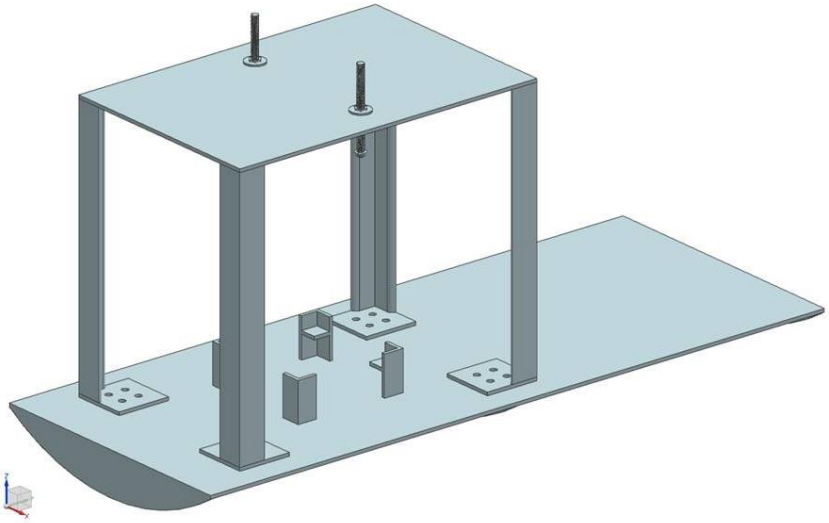

Figure 3.3: CAD Model of the Test Stand

### 3.2.3 Cradle

A cradle (Figure 3.4) is used to adjust the contact between the heating block and the test sections. Aluminum T-6061 was selected as the cradle's material for cost and machinability purposes when compared to stainless steel. Two ports were machined to allow the connection to the stand using two steel bolts. A 3.2 mm slit was machined along the top of the cradle to allow for thermocouple placement.

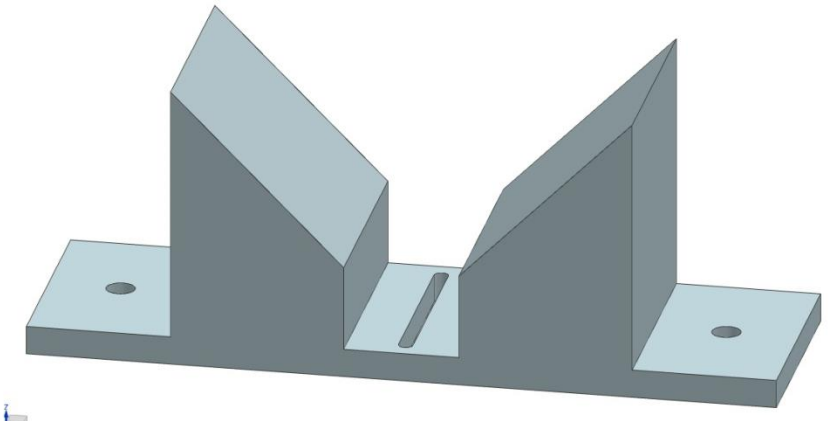

Figure 3.4: CAD Model of the Aluminum Cradle

### 3.2.4 Test Section Cooling Channels

The test sections in this experimental study refer to the sections used to characterize the cooling properties of $LCH_4$. The main reason for choosing copper as the material for the test sections is that copper is known as the industry standard for cooling channel wall material due to its highly conductive thermal properties [8]. More specifically, the alloy selected to manufacture the test sections is copper C18200 due to the relatively high thermal conductivity and higher strength attributes as compared to copper alloys with higher copper content. Every channel has six ports distributed axially where thermocouples are placed to measure the channel wall temperature. All channels presented in this study have a channel wall thickness of 1.3 mm. Inspired by the need to test cooling channels with different features, the HHFTF features the ability to substitute test sections in a modular approach without the need to alter the heating block. A test section model is shown in Figure 3.5 specifying the exit length, the main heated segment, and the exit length locations. Cooling channels representing milled channels contain an extra transition entry section to smooth the flow of $LCH_4$ as it enters the entry region.

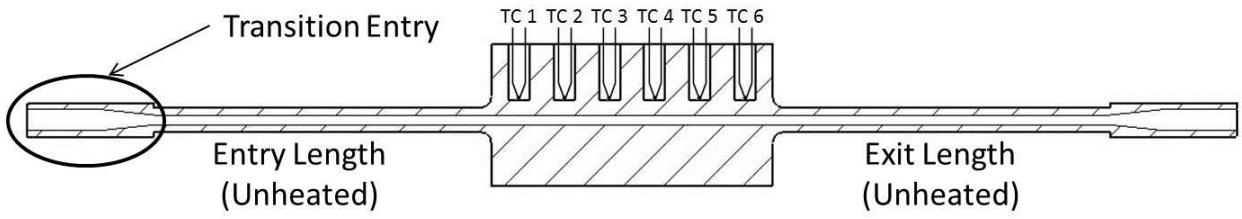


Figure 3.5: Test Section Model

All the test sections presented in this study represent milled cooling channels. The first test section contains a cooling channel with a rectangular cross section that has a width of 1.8 mm and a height of 4.1 mm. This test section was developed at NASA White Sands Test Facility (WSTF), and it is a subscale representation of a cross-section of a channel in NASA Project Morpheus' HD3 regen cooling jacket design. More specific, such location of interest is right after the combustion chamber upon entering the nozzle. The rectangular channel is shown in Figure 3.6.

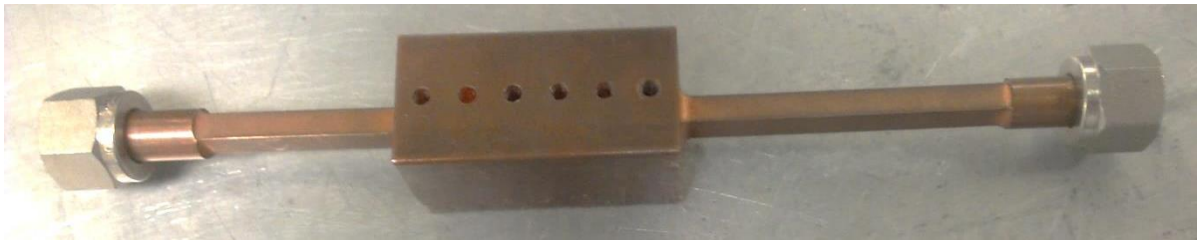

Figure 3.6: Rectangular channel with cross section of 1.8 mm x 4.1 mm

The remaining four test sections contain a cooling channel with a square cross section of 3.2 mm x 3.2 mm. The geometry and dimensions were chosen due to machining limitations and entry length requirements. One of the square test sections has a smooth cooling channel while the remaining three have rough cooling channels. As mentioned before, the purpose of these square channels is to study the effects of surface roughness and since the test sections represent milled channels, the roughness values were selected with respect to common milling surface finishes as seen in [5]. The three rough test sections have surface finishes of 0.8, 3.2, and 6.4 microns (μm) based on the arithmetic mean value scale ($R_a$). The smooth test section will serve as a basis of comparison of the effects of surface roughness. Figure 3.7 shows an image representative of all the square channels presented in this study.

Figure 3.7: Square channel with cross section of 3.2 mm x 3.2 mm

# Chapter 4: Methane Condensing Unit

## 4.1 1st Generation Condensing Unit

The HHFTF incorporates a methane condensing sub-system known as the Methane Condensing Unit (MCU) in order to provide the system with $LCH_4$. The MCU is the product of a progressive effort aimed to develop a system capable of condensing methane in-house. A first generation unit was developed as a proof of concept system that produced up to 1 L of $LCH_4$ in a vacuum insulated flask. Figure X shows the setup of the 1st generation condensing unit. It utilized a shell and coiled tube heat exchanger where liquid nitrogen ($LN_2$) flowed through the coil inside the condenser flask while $GCH_4$ was fed to the flask at 34.4 kPa. In order to calculate the amount of condensed methane, the flask was placed on a weigh scale. Also, a type E thermocouple was placed at a defined height to indicate the presence of 1 L of $LCH_4$ when the saturation temperature was reached.

Figure 4.1: 1st Generation MCU Setup

## 4.2 2nd Generation Condensing Unit

After successfully proving the shell and coil heat exchanger concept with the 1st generation unit, a 2nd generation unit was developed at the cSETR. With the need of supplying $LCH_4$ to several

experimental setups throughout the cSETR laboratory, the 2nd generation MCU was designed as a mobile unit. This unit contains two separate tanks as shown in Figure 4.2. The top tank is a stainless steel cylinder that was machined to place a coil inside through which $LN_2$ flowed. This tank is able to condense approximately 2 L of $LCH_4$. Due to machining done to customize the condensing tank, safety issues prohibited pressurizing the tank to relatively high pressures. For this reason, the bottom tank was used as the run tank which could be pressurized to the required pressures. Therefore, this condensing unit required a transfer process from the condensing tank to the run tank; unfortunately, the transfer process created issues dealing with vapor lock and $LCH_4$ losses. Once sufficient methane was condensed and transferred to the bottom tank, helium was used to pressurize the run tank in order to supply the HHFTF with $LCH_4$. Coils are placed around the tanks where $LN_2$ flows to chill the outer walls. The modified condensing tank is shown in Figure 4.3(a) while the run tank is shown in Figure 4.3(b). All components and gas tanks are placed on a stainless steel cart. The condensing system involves several fluids and components for proper delivery to the HHFTF such as liquid nitrogen (LN2), GCH4 and LCH4, gaseous helium (GHe), cryogenic manual and solenoid valves, pressure relief valves, check valves, thermocouples, pressure transducers, and a flow meter. To check methane temperatures in the tank, five ungrounded sheathed type E thermocouples are placed inside ports located vertically along the tank as shown in Figure 4.3(a). The purpose of the 2nd generation MCU design was to further prove the ability to condense methane at increased volumes. In addition, the design of this system allowed the possibility to attain the transient heat transfer characteristics when integrated to the HHFTF. However, steady state data was not acquired with the 2nd generation unit.

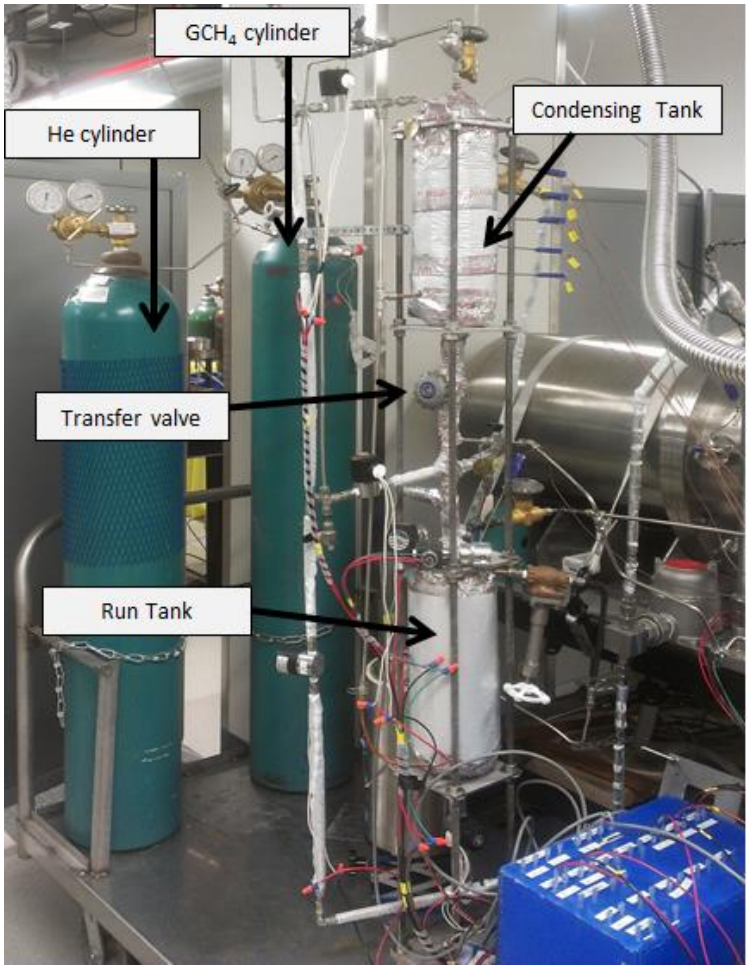


Figure 4.2: 2nd Generation MCU Setup


Figure 4.3: (a) 2.2 L Insulated Condensing Tank Equipped with Five Thermocouples. (b) Run Tank Wrapped with Copper Coil.

## 4.3 3rd Generation Condensing Unit

In order to provide the system with sufficient $LCH_4$ to acquire steady state wall temperature data a 3rd generation condensing unit was developed at the cSETR. This was achieved by rating a 13 L stainless steel double ended cylinder (shown in Figure 4.4) to approximately 3.4 MPa which allows it to serve as both the condensing and run tank at cryogenic temperatures. With this, the issues associated with a transfer process as seen on the 2nd generation condensing unit were eliminated in this design. Another similar characteristic to the previous unit is that the 13-L MCU is placed on a mobile cart for transportation purposes. In addition, the 3rd generation unit also involves several fluids and components for proper delivery to the HHFTF such as $LN_2$, $GCH_4$ and $LCH_4$, GHe, cryogenic manual and solenoid valves, pressure relief valves, check valves, thermocouples, pressure transducers, and a flow meter. The tank is configured as a shell and coil heat exchanger with a 316 L stainless steel outer shell. An 18.3 m coil made of 6.35 mm outer diameter (OD) stainless steel tubing is placed inside the tank; as $LN_2$ flows through this inner coil, methane condenses in the tank. Additionally, the tank is wrapped with 30.5 m of 6.35 mm OD copper tubing through which $LN_2$ flows to cool the tank walls; furthermore, the copper tubing is covered with three 6.35 mm thick layers of cryogenic insulation. To check methane temperatures in the tank, eight ungrounded sheathed type E thermocouples are placed inside ports located vertically along the tank. In addition, a thin film cryogenic pressure transducer is located at the top of the tank. The results presented in this study were achieved using the 3rd generation MCU. Figure 4.4 shows the integration of the 3rd Generation MCU to the HHFTF.

Figure 4.4: 3rd Generation MCU Condensing/Run Tank

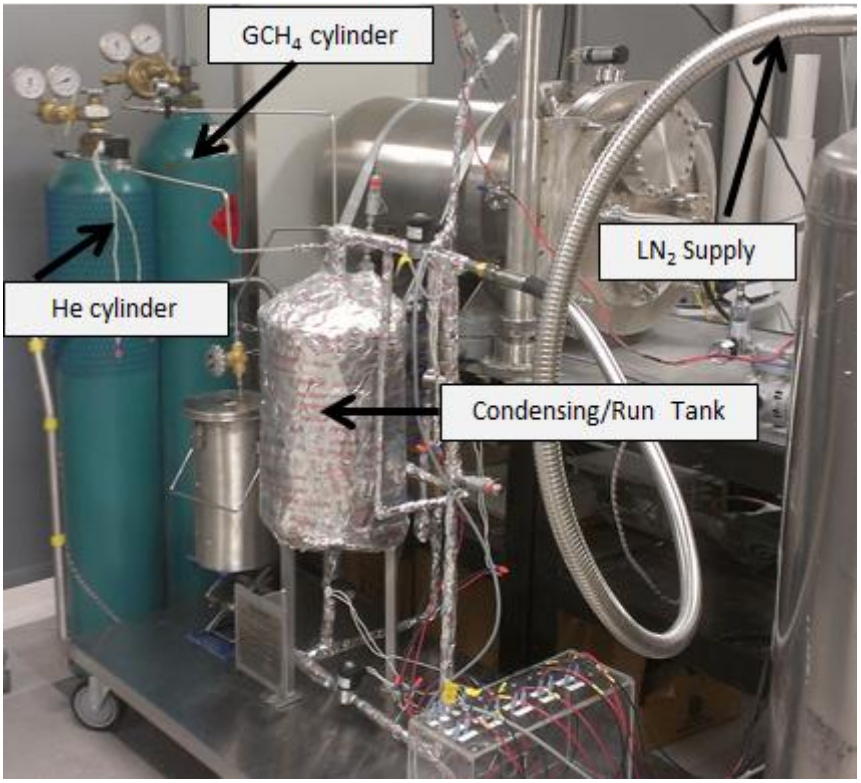


Figure 4.5: 3rd Generation MCU Setup

# Chapter 5: System Integration and Components

## 5.1 System Integration

The complete experimental setup used in this study integrates the MCU to the HHFTF, as shown in Figure 5.1. The full system setup consists of several components that have been verified to operate at the required conditions for this study; that is, the system operates under temperatures ranging from -200°C to 650°C, pressures up to 2.4 MPa, and vacuum levels around $2.5 \times 10^{-2}$ torr. The system also uses components to measure different parameters as well as to acquire and record data for further analysis.

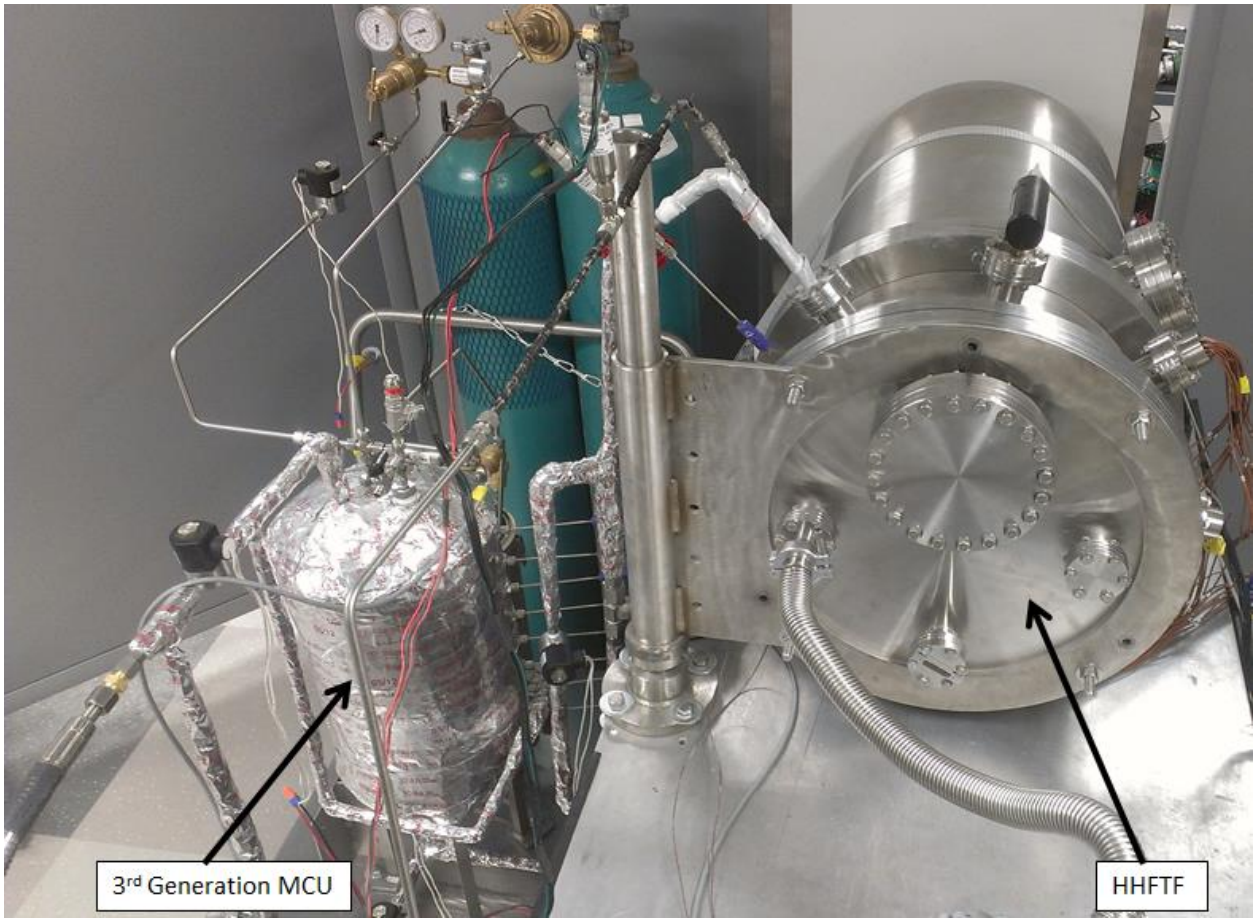


Figure 5.1: Integration of the 3rd Generation MCU to the HHFTF

## 5.2 System Measurements

The system includes components that allow measurement of three important parameters of this study: flow rate, temperature, and pressure. These components comprise a large part of the data analysis and redlines incorporated into the test procedure. Next, the measurement components are described. A more detailed description of the instrumentation is included in the Appendix.

### 5.2.1 Temperature Measurement

Several types of devices are used to monitor temperatures in the system. To measure the block temperature, four Omega Nextel™ insulated type K thermocouples are used; they offer the advantage of measuring temperatures in small areas in a confined space. Additionally, six exposed tip Type E thermocouples are used to measure the wall temperature at the test section ports. Two ungrounded sheathed type E thermocouples measure the fluid bulk temperatures. Moreover, eight ungrounded sheathed type E thermocouples measure the temperature of methane in the condenser unit. Figure 5.2 shows the different types of thermocouples used in this experiment.

Figure 5.2: Omega Nextel™ Insulated Type K Thermocouples (left), and Omega Ungrounded Sheathed Type E Thermocouples (right)

### 5.2.2 Pressure Measurement

To measure the system pressures, three thin film cryogenic pressure transducers are utilized. One of the pressure transducers is located at the top of the condenser tank. This transducer acts as a set point when running the experiments at the desired tank pressures based on the test matrix. The remaining two

pressure transducers are installed upstream and downstream of the test sections and are used to measure the pressure drop across the channel. This also aids in the correlation of the mass flow rate of the fluid further discussed in the results section. In addition, the components used in the HHFTF to measure vacuum levels in the chamber include a pirani vacuum gauge controller, and a convection-enhanced pirani sensor. Figure 5.3 shows the pressure measuring devices used in the system.


Figure 5.3: (a) Omegadyne Thin Film Cryogenic Pressure Transducer. (b) Pirani Vacuum Gauge Controller. (c) Convection-Enhanced Pirani Sensor

### 5.2.3 Flow Rate Measurement

A turbine flow meter manufactured by Hoffer Flow Controls, Inc. is installed in the propellant line just upstream of the cooling channel section. The turbine spins at a certain rpm depending on the density and velocity of the fluid. The flow meter used in this study has been calibrated by the vendor to be used specifically with $LCH_4$. It is rated to a range between 0 to 17 Liters per minute (Lpm). Figure 5.4 shows the flow meter integrated to the HHFTF propellant line.

Figure 5.4: Hoffer Turbine Flow Meter Installed in the HHFTF Propellant Line

### 5.2.4 Data Acquisition System

A data acquisition (DAQ) system has been setup in order to monitor the system parameters as well as to record data required for further analysis. Two NI 9213 16-Channel thermocouple input modules connected via USB to the computer used for the experiment are used to record all temperature measurements associated with the HHFTF and MCU systems. The pressure transducers are connected to a SCC-68 unit which is in turn connected to a NI PCI-6533. Each pressure transducer is connected to a 1/8 DIN process meter and controller. The process meters are used for signal conditioning and offer added convenience as the display can be seen by the personnel monitoring the pressures in the system. Figure 5.5 displays the DAQ devices used in the system.


Figure 5.5: From Right to Left: NI PCI-6533, NI SCC-68, NI 9213 and Omega 1/8 DIN Process Meter (Bottom)

The graphical user interface (GUI) used to view the real time output signals from the DAQ system is shown in Figure 5.6. The GUI shows the measurements from the test section wall temperatures, heating block temperatures, condensing tank fluid temperatures, as well as run tank and in-line pressures. A switch labeled “record on” is activated to begin recording data when the test is ready to begin.

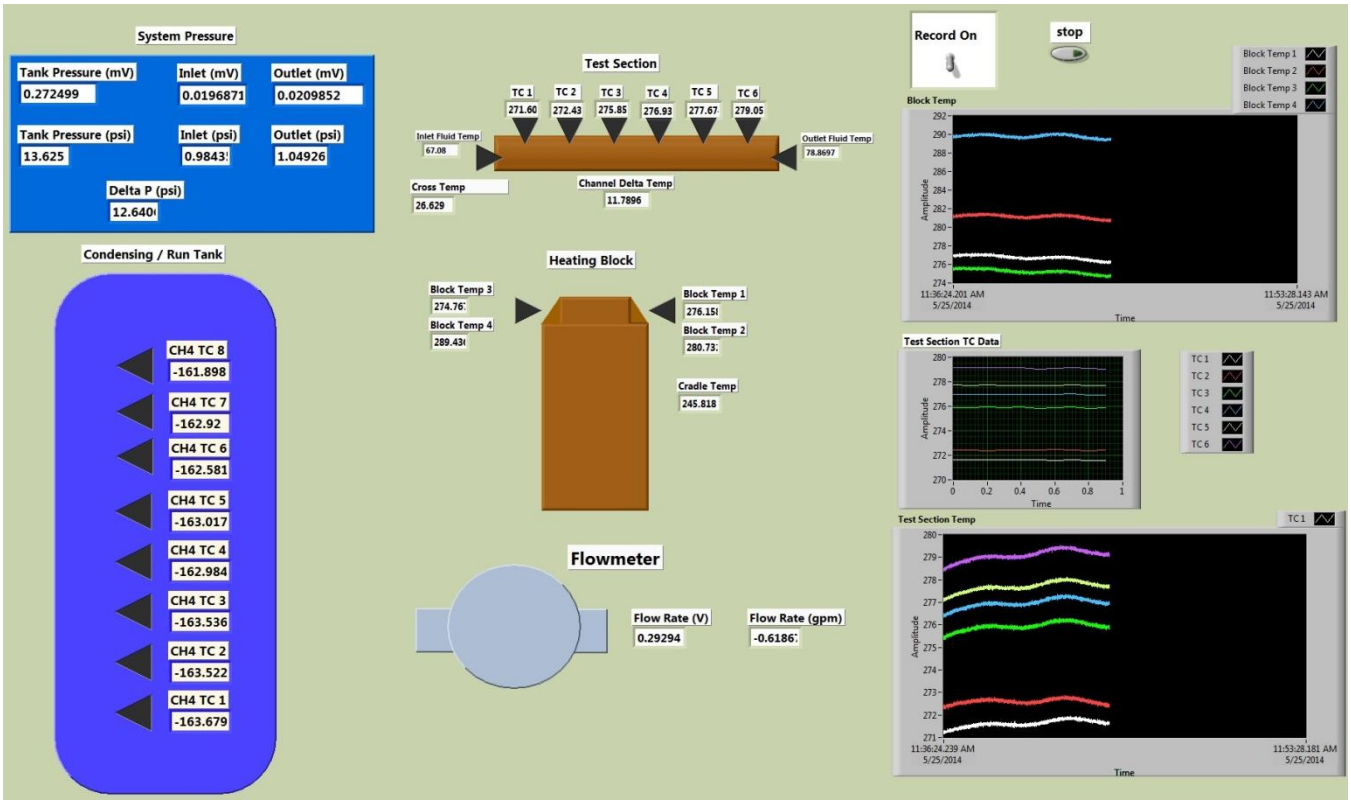


Figure 5.6: NI LabVIEW 13.0 HHFTF/MCU Graphical User Interface

## 5.3 Valves

The system employs various types of valves which have different functions such as regulating back pressure, and controlling the flow path of the fluids used in the experiment. Six normally closed solenoid valves are used for control during a test sequence. These 12 V solenoid valves (shown in Figure 5.7) are rated for cryogenic use and basically control the flow path of the fluids involved.

Figure 5.7: Gems Sensors D-Cryo Series Solenoid Valves

Also, cryogenic manual valves made by Rego Products, shown in Figure 5.8, are mainly used to generate back pressure for the flow of $LN_2$ through the condenser coils so that it prevents over-chill of the system or decreasing the temperature of $LCH_4$. Similarly, a cryogenic needle valve made by Dragon Valves Inc., shown in Figure 5.9, is installed downstream of the test section to provide adequate control of the flow rate of $LCH_4$ passing through the cooling channel.


Figure 5.8: Rego Cryogenic Globe Valve

Figure 5.9: Back-Pressure Regulating Needle Valve

Moreover, non-cryogenic quarter turn valves, shown in Figure 5.10 (a), are used to control the flow path for vacuum pumps, and the supply of gaseous methane and helium into the condenser/run tank. Furthermore, pressure relief valves, shown in Figure 5.10 (b), are installed in case the lines over pressurize due to trapped cryogenics. Also, cryogenic check valves are used in the MCU to prevent back flow of fluids. Figure 5.11 shows an image of a cryogenic check valve.

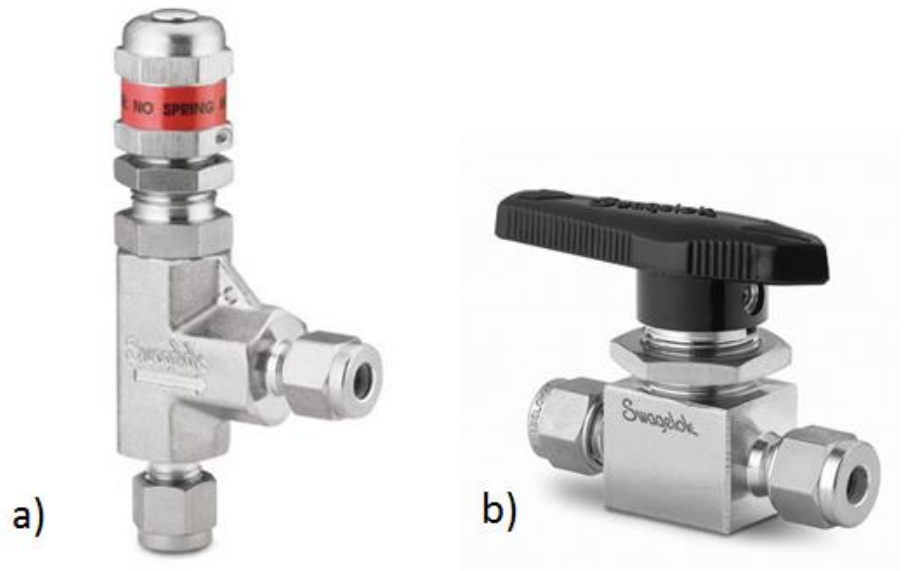


Figure 5.10: (a) Swagelok Pressure Relief Valve. (b) Swagelok Quarter-Turn Valve

Figure 5.11: Generant Cryogenic Check Valve

## 5.4 Fluids

As mentioned before, this experiment involves the use of fluids such as $LN_2$, $GH_4$, $LCH_4$, and He. The gaseous methane supplied to the condenser tank is C.P. (chemically pure) grade 99.0% methane; this grade of methane was chosen to prevent inconsistencies in the data due to the impurities in lower grade methane. In addition, helium is used to pressurize the $LCH_4$ in the condenser tank and force it through the test section cooling channel; more specifically, industrial grade 99.0% helium is used in this experiment. Helium was chosen due to its inert characteristics and because it has a significant lower saturation temperature than methane eliminating the risk of condensing the pressurant gas; that is, helium's saturation temperature is 1.2 K at ambient conditions. Moreover, the fluid used in the heat exchanger to condense methane is $LN_2$. It is also used to chill the system lines before $LCH_4$ flows through the channel.

## 5.5 Vacuum Pumps

Risk mitigations include the evacuation of air in all propellant lines and condensing tank. This ensures that $CH_4$ does mix with any surrounding oxygen preventing a flammable environment. In addition, the copper test section is heated to temperatures such that an oxidation layer may form along the inner walls of the channel creating dissimilar surfaces for each test if vacuum is not pulled. Vacuum is pulled through the propellant lines and test section with a piston powered vacuum pump. Typical vacuum levels in the lines reach values of about 6.9 kPa. Figure 5.12 shows the line vacuum pump.


Figure 5.12: Rocker 300 Vacuum Pump

Also, a scroll vacuum pump is utilized to pull vacuum in the altitude chamber to minimize convective losses to simplify data analysis. Additionally, it is also used to prevent oxidation from forming on the heating block as well as the contact surfaces between the block and test section which would affect the heat transfer between the two surfaces. The average vacuum levels reached in the chamber go as down as $5.0x10^{-2}$ torr. The chamber vacuum pump is shown in Figure 5.13.


Figure 5.13: Edwards XDS5 Scroll Vacuum Pump

## 5.5 Electrical Components

The electrical system of this study encompasses components used to power the six actuated valves, the three pressure transducers, and the eighteen heating cartridges. The cartridge heaters used to heat the block are 400 W-120 VAC heaters. The cartridges are controlled by a series of solid state relays (SSR). The wiring schematic of the heaters to SSR is provided in the Appendix. The SSR are manually powered by a switch connected to a DC power supply of 5 VDC. When the SSRs are triggered by the switch, current is allowed to flow through the heating cartridges. A complete electrical schematic pertaining to the cartridge to SSR connection is shown in the Appendix. Figure 5.14 (a) shows the cartridge heaters while Figure 5.14 (b) illustrates heaters being inserted into the block. Figure 5.15 shows an example of the SSRs used in the experiment.

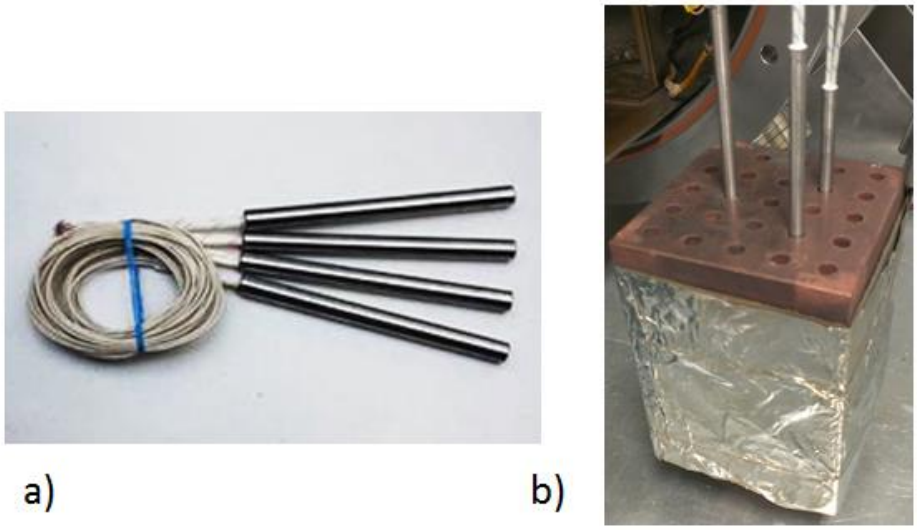


Figure 5.14: (a) Gordo Sales Cartridge Heaters. (b) Heaters Inserted into the Block


Figure 5.15: Omega Solid State Relays

The power system used two Extech Quad Output DC power supplies (Figure 5.16) connected to standard 120 VAC power outlets. The power supplies offer the capability of adjusting the voltage and current levels that the actuated valves and pressure transducers require. The valves require a voltage level of 12 VDC and draw approximately 1.3 A, while the pressure transducers are activated by an excitation voltage of 10 VDC.


Figure 5.16: Extech Quad Output Power Supply

## 5.6 Test Procedure

The test procedure can be separated into three main steps: the condensation of $LCH_4$, the heating of the block and the flow of $LCH_4$ through the test section. It should be noted that the condensation of methane and the heating of the copper block occur simultaneously. A step-by-step procedure and the fluid schematic are included in the Appendix. Nonetheless, a brief overview of the experimental procedure is covered in the following sections.

### 5.6.1 Methane Condensation

As mentioned before, vacuum must be pulled in the system lines and tank before initiating the condensation process to prevent any flammable environment. Once this happens, the outer and inner coils of the condenser tank are chilled with $LN_2$ until the tank temperatures measure approximately 170 K. Then, the condensing tank is pressurized with gaseous methane while $LN_2$ flows continuously through the coils. This goes on until sufficient methane has been condensed. On average, it takes approximately 60-90 minutes to condense about 13 L of $LCH_4$. As mentioned previously, the level of $LCH_4$ in the tank is monitored with the fluid temperature measurements in the tank.

### 5.6.2 Block Heating

As the condensation process takes places, the heating process is also occurring. Before powering the cartridge heaters to raise the temperature of the block, vacuum is pulled in the altitude chamber to prevent convective losses and oxidation related issues. The heating cartridges are controlled manually using switch as mentioned before. The heating of the block is gradual. To prevent heater failure, the cartridge heaters cannot be powered for more than 20 s continuously. It was found that cycling the heaters 3 seconds on and off results in the heaters lasting more than 6 months. This on/off cycle translates into the temperature of the block increasing with a ramp rate of about 0.3°C per second.

### 5.6.3 Methane Flow Test

Once sufficient methane has been condensed and the desired block temperature has been reached based on the test matrix, helium is allowed into the tank to pressurize the $LCH_4$, then the lines and test section cooling channel are chilled with $LN_2$ until the required temperature is reached also based on the test matrix. All the actuated valves and the switch that powers the heaters are installed in a control box located near the computer monitors so that the personnel in charge can control the switches and monitor the test parameters with the aid of the GUI. Figure 5.17 shows the control box housing where all the switches are installed.

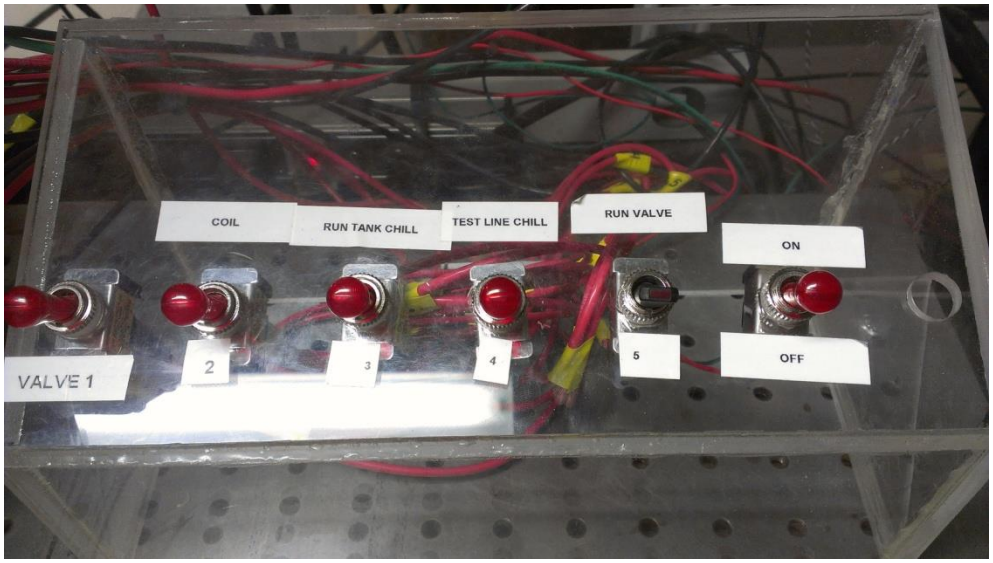


Figure 5.17: Control box containing all system manual switches to operate valves and heaters

Subsequently, the data acquisition system is set to record all the temperature, pressure, and flow rate data. Finally, pressurized $LCH_4$ is allowed to flow through the test section cooling channel. One member of the research team is in charge of monitoring the test via the GUI as well as controlling the valves while another member is in charge of regulating the pressure of helium to maintain a constant methane pressure. A sudden drastic increase in the wall and channel fluid temperatures indicates the depletion of methane. At this point the recording of data and the flow of helium are stopped.

### 5.6.4 Post-Test Procedure

All the cryogenic methane that flows through the channel is captured and vented in a non-flammable environment using a cryogenic dewar connected to a vent system. The system is purged with helium to evacuate any remaining methane in the tank and lines. All manual valves are opened to prevent trapping cryogenics into the system and over pressurizing the lines. In case of possible over pressure, pressure relief valves set to activate when pressures reach 2.4 MPa are installed in the MCU. Although vacuum is pulled in the lines and chamber after every test to prevent oxidation build up, the components are frequently checked and cleaning of surfaces is done on the heating block and test section if needed. Moreover, to check heater functionality, the resistance of each cartridge heater is measured using a voltmeter. In addition, thermocouples are also tested before each experiment by measuring the temperature of known substances such as water ice.

# Chapter 6: Results and Discussion

## 6.1 Test Matrix Development

The test conditions incorporated into each test matrix are focused primarily on the block temperature and test pressure. The test pressures are directly related to flow rates and subsequent Reynolds numbers. The flow rates are calculated by performing a calibration test relating the pressure difference (from the tank to the channel inlet) to the flow rate from the turbine flow meter. With both of these parameters, a test matrix is generated for each cooling channel tested.

### 6.1.1 Flow Rate Calibration

Mass flow rate of $LCH_4$ during a given test was determined by a calibrated delta-pressure measurement. The flow meter was not used to measure $LCH_4$ flow rate real-time because use of the turbine flow meter during a test did not permit wall temperatures to reach steady state. This is because a significant amount of $LCH_4$ is wasted in cooling the flow meter. $LN_2$ was not used to chill the flow meter because the initial water hammer and cryogenic boil off could damage the flow meter by over-spinning the turbine. The calibration method used dedicated $LCH_4$ flow rate test cases to measure pressure difference between the tank and the inlet of the test section. This method eliminates the need to perform a calibration test for every test section (i.e., the calibrated pressure drop was not performed across the test article). Figure 6.1 shows the methane flow rate calibration relating the mass flow rate to the pressure drop. Density for the $LCH_4$ was calculated using REFPROP [18], with the state definition at the test article inlet pressure and inlet temperature.

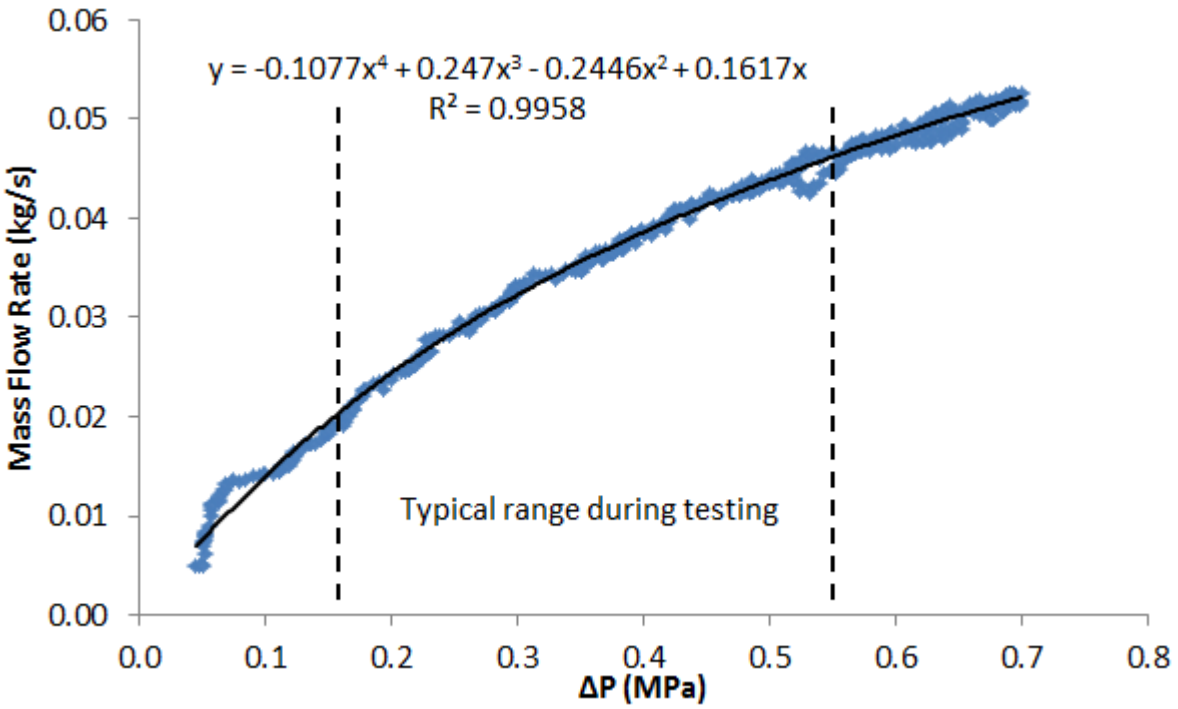


Figure 6.1: Methane Flow Rate Calibration Curve for Pressure Drop from Tank to Test Article Inlet

### 6.1.2 Test Matrices

The parameters which were consistent for each test are the initial inlet temperature and tank pressures. The initial inlet temperature is approximately -165°C and it is achieved by flowing $LN_2$ through the test article. This temperature was chosen to avoid losing any $LCH_4$ at the beginning of the test which would risk reaching steady state conditions. The tank pressures range from 1.0 MPa to 2.1 MPa. Table 6.1 shows the test matrix for the 1.8 x 4.1 mm cooling channel. Table 6.2 shows the test matrix for the 3.2 mm x 3.2 mm cooling channels (smooth and rough).

Table 6.1: Test Matrix for the 1.8 mm x 4.1 mm Cooling Channel

| 1.8 mm x 4.1 mm Cooling Channel | | | | | |
|---|---|---|---|---|---|
| Pressure (MPa) | Block Temperature (°C) | | | | |
| 1.03 | 200 | 250 | 300 | 350 | 400 |
| 1.38 | 200 | 250 | 300 | 350 | 400 |
| 1.73 | 200 | 250 | 300 | 350 | 400 |
| 2.07 | 200 | 250 | 300 | 350 | 400 |

Table 6.2: Test Matrix for the 3.2 mm x 3.2 mm Cooling Channels

| 3.2 mm x 3.2 mm Cooling Channels | | |
|---|---|---|
| Pressure (MPa) | Block Temperature (°C) | |
| 1.03 | 200 | 275 |
| 1.55 | 200 | 275 |
| 2.07 | 200 | 275 |

## 6.2 Data Analysis

For data analysis, two primary measurements taken from the test section are temperatures and pressures. A more descriptive image showing the channel wall thermocouple arrangement can be seen in Figure 6.2. The surface or skin temperature is measured by six exposed tip type E thermocouples along the channel and 8.3 mm apart. Before the vacuum chamber is sealed, proper thermocouple-to-channel surface contact is checked by testing continuity between the thermocouple and the channel surface using a multi-meter.

Figure 6.2: Channel wall thermocouple arrangement

In addition, the fluid bulk temperature measurements are taken by two ungrounded sheathed type E thermocouples. The fluid temperature measurements act as a method for determining the start of $LCH_4$ entering the channel and the moment when the $LCH_4$ supply has finished. Figure 6.3 is a representative illustration showing the channel wall and fluid thermocouple arrangement. The inlet fluid thermocouple was placed just before the entry length to avoid any obstruction to the flow of $LCH_4$ (i.e., preventing the flow of $LCH_4$ from fully developing). As mentioned before, pressure transducers are also placed at the

inlet and outlet of the test section. The fluid properties are evaluated at the bulk temperature and channel average pressure due to the relatively large difference in wall temperature and bulk temperature [19].

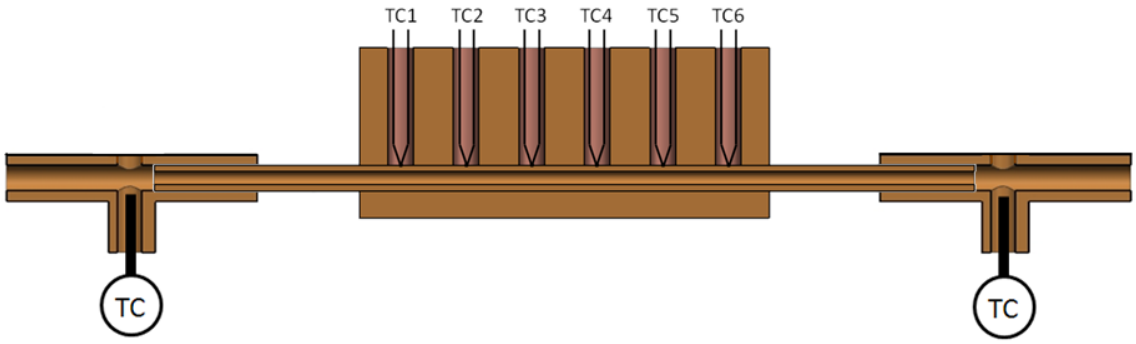


Figure 6.3: Wall and Fluid Thermocouple Placement

The data obtained from the tests was used to develop correlations for Nusselt number, *Nu*, and Reynolds Number, *Re*. Total rate of heat transfer to the fluid was calculated based on the mass flow rate of the fluid, $\dot{m}$, specific heat, *Cp*, and temperature change from fluid inlet to outlet, ($T_{out} - T_{in}$), as in Eq. (6.1) [20]. Surface heat flux, $\dot{q}_s$, was determined using the test section coolant channel wall surface area, $A_s$, as in Eq. (6.2).

$$\dot{Q} = \dot{m} C_p (T_{out} - T_{in}) \tag{6.1}$$

$$\dot{q}_s = \frac{\dot{Q}}{A_s} \tag{6.2}$$

Mass flow rate, $\dot{m}$, was determined from the pressure-drop calibration for mass flow rate (described above). The resultant heat flux is then used to calculate the local heat transfer coefficient, $h_x$, shown in Eq. (6.3).

$$h_x = \dot{q}_s / (T_s - T_m) \tag{6.3}$$

Where $T_m$ is the mean fluid temperature and is calculated using Eq. (6.4).

$$T_m = T_{in} + \frac{\dot{q}_s p}{\dot{m} C_p} x \tag{6.4}$$

Where $T_{in}$ is the channel inlet fluid temperature, $p$ is the perimeter of the tube, and $x$ is the axial location along the heated segment of the cooling channel. With $h_x$, an average heat transfer coefficient $h_L$ was calculated using Eq. (6.5).

$$h_L = \frac{1}{L}\int h_x dx \tag{6.5}$$

The measured $Nu_L$ is then calculated using Eq. (6.6) where $k$ is the fluid thermal conductivity.

$$Nu_L = \frac{h_L D_h}{k} \tag{6.6}$$

Shown in Eq. (6.7), bulk Reynolds number was defined using the fluid density, $\rho$, fluid viscosity, $\mu$, test article hydraulic diameter, $D_h$, and bulk velocity, $v$, which is calculated from the $\dot{m}$, $\rho$, and cooling channel cross sectional area.

$$Re = \frac{\rho v D_h}{\mu} \tag{6.7}$$

All the state properties such as $\rho$, $\mu$, $Cp$, and $k$, were calculated with REFPROP [18] at the average fluid pressure, $P_{avg}$, where $P_{avg} = ½ (P_{in} + P_{out})$, and bulk temperature, $T_b$, where $T_b = ½ (T_{in} + T_{out})$. $T_{out}$ is the fluid temperature at the channel outlet.

### 6.2.1 Measurement Uncertainty

The determination of the maximum uncertainty for the data points collected pertains mainly to accuracies of the components reported by the vendors. Using Table 6.3, which shows the error associated with each parameter, the propagation of uncertainty shown in Eq. (6.8) is used to find the combined error for each parameter. This error is the resultant effect for the measured quantities from the flow meter, temperature, and pressures. The error in mass flow rate measurement is directly influenced by the flow meter during the calibration tests and the resultant pressure differential relationship attained during the actual $LCH_4$ test runs. Similarly, the heat transfer coefficient error stems from the temperature measurements associated with the channel wall and fluid thermocouples. The fluid state

properties are evaluated using REFPROP [18] which includes an accuracy of ±0.2 also affecting mass flow rate. Taking into account these values, the combined uncertainty for $Nu_L$ is estimated to be +/- 6.2%.

$$(U_{cal.}) = \sqrt{\sum \left( \frac{\partial f(Calculated)}{\partial Variable} Error_{variable} \right)^2} \tag{6.12}$$

Table 6.3: Measurement Accuracy Associated for Each Component

| **Parameter** | **Error %** |
|---|---|
| Turbine Flow Meter | ± 0.10 |
| Pressure Transducers | ± 0.25 |
| Thermocouples | ± 1.00 |
| REFPROP (Fluid Properties) | ± 0.20 |
| Pressure Differential | ± 0.35 |
| Temperature Differential | ± 1.40 |
| Mass Flow Rate | ± 1.23 |
| Local Heat Transfer Coefficient | ± 2.42 |
| Heat Flux | ± 2.64 |
| Measured Nusselt Number | ± 6.20 |

## 6.3 Steady State Data

Analysis of the steady state data only considers the portion of data indicating steady state wall and bulk temperatures. Figure 6.4 shows a test run for the 1.8 x 4.1 mm rectangular channel. In Figure 6.3 “TC 1 – TC 6” indicate the wall temperature measurements being “TC 1” the closest to the channel inlet. “Outlet” and “Inlet” refer to the methane temperature at the outlet and inlet of the channel, respectively. The test is initiated when methane flows into the test section (e.g., at Time = 0 s in the example provided). A 10-second steady state average for all the temperature measurements is taken for each test; in the example shown in Figure 6.4, this occurs at about 190-200 s into the test indicated by the black dashed lines. Methane is depleted at about 210 s into the test as indicated by the red dashed line. Each test case includes similar temperature plots analyzed in this manner.

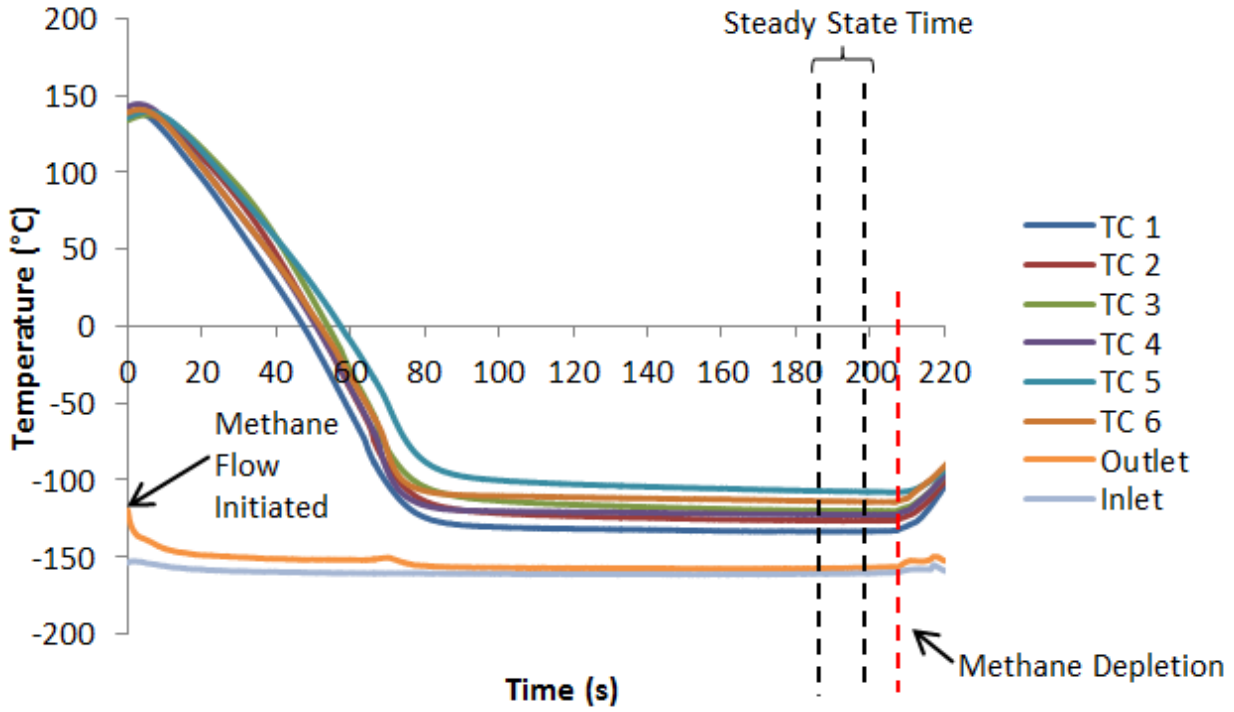


Figure 6.4: Steady State Temperature Profile Example, 1.8 mm x 4.1 mm Channel

### 6.3.1 Rectangular Channel, 1.8 mm x 4.1 mm

For the cooling channel with the 1.8 mm x 4.1 mm cross section 35 data points were collected. Figure 6.5 shows example test measurements of the six wall and fluid temperatures. Note that the "Steady state" time is when the wall temperatures are averaged for the data points.

The steady state measured Nusselt number versus bulk Reynolds number plot is shown in Fig. 6.6. This figure shows that the range of Nusselt numbers is between 40 and 325 and Reynolds numbers range between 68,000 and 131,000. The data points showed that in some tests, the channel wall was cooled more effectively than others; that is, in some tests, the channel wall temperatures were below 0°C. Figure 6.5 (a) shows an example of a "hot-wall" test and Fig. 6.5 (b) shows an example of a "cold-wall" test. The data was classified in three categories; cold-wall, hot-wall, and mixed. Cold-wall denotes the data where all channel wall temperatures were below 0°C; hot-wall denotes the data points in which all channel wall temperatures were above 0°C. Finally, mixed indicates the data where there was a mix of channel wall temperatures above and below 0°C. The differences between hot-wall data and cold-wall measurements suggested that there could be a film-boiling phenomenon in the data. Since

these experiments were all conducted with $LCH_4$ that had been cooled with $LN_2$, the inlet condition to the test article was always sub-cooled. Any film-boiling phenomenon measured in the test article would be classified as "sub-cooled film-boiling". The Nusselt numbers represent the convective component of the heat flux, as calculated by Eq. (6.1) and Eq. (6.2) (i.e., heat used in boiling is not measured or included in the Nusselt number term).

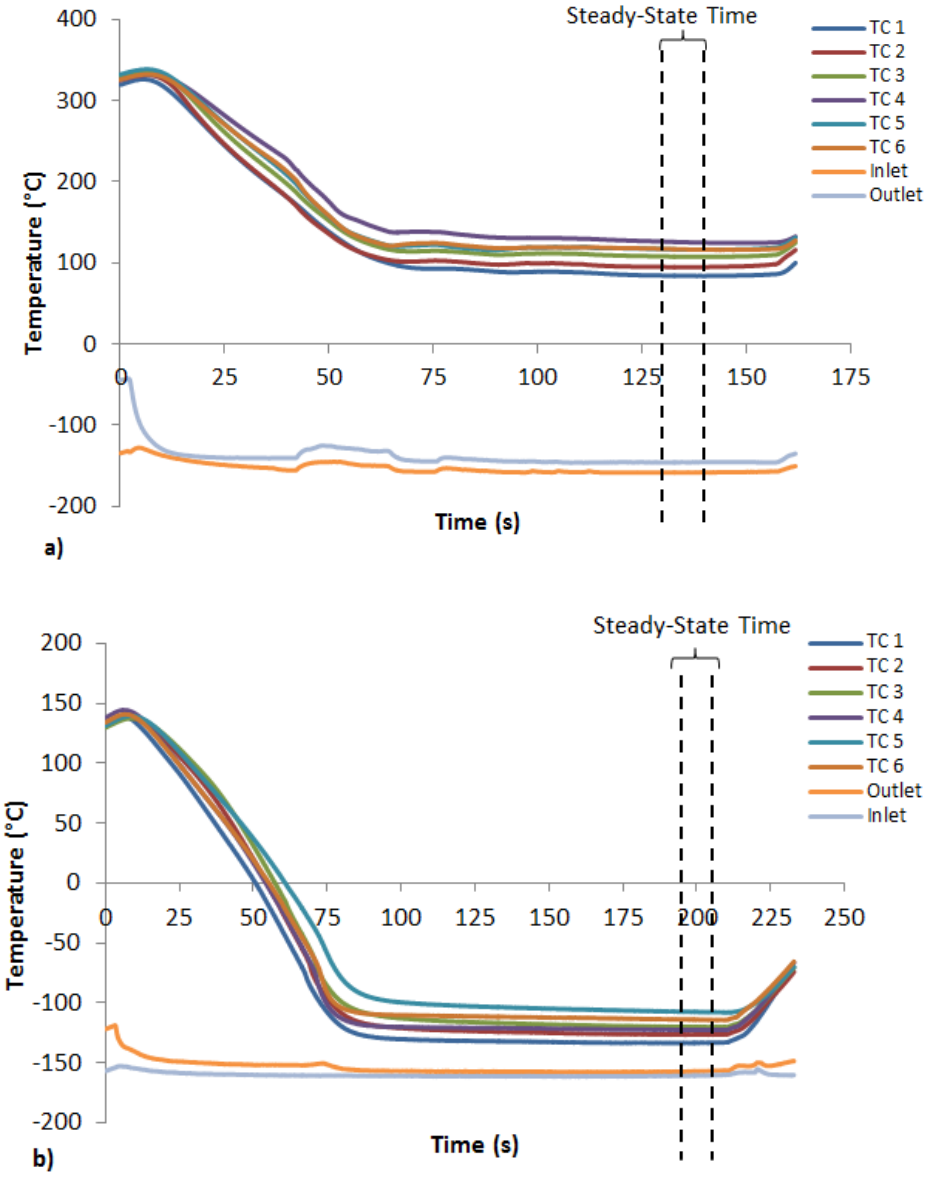


Figure 6.5: Example Test Measurements of the Six Wall and Fluid Temperatures as a Function of Time, 1.8 mm x 4.1 mm channel. (a) "Hot-Wall" Test Example. (b) "Cold-Wall" Test Example.

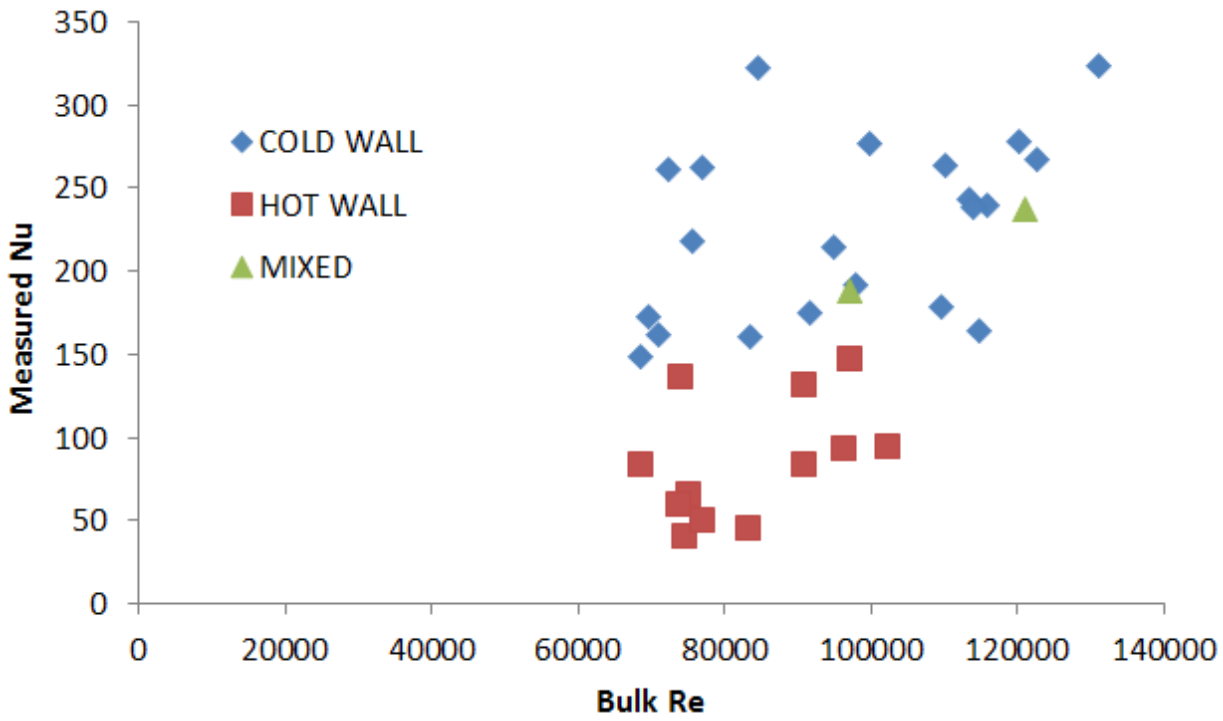


Figure 6.6: Measured Convective Nusselt Number as a Function of Bulk Reynolds Number, 1.8 mm x 4.1 mm test article

Figure 6.7 shows the heat flux versus average wall temperature minus saturation temperature where the modes of heat transfer can be observed; more specifically, the non-boiling and film-boiling regions. In film-boiling regime, all six wall temperature measurements read "hot" together, indicating that the critical heat flux (CHF) onset occurs in the 5.1 mm prior to the first wall thermocouple. It should be noted that the heat flux values were calculated using the conservation of energy equation for the steady flow of a fluid in a tube as in Eq. (6.1). This equation is only valid for the convective heat transfer; however, it is used as an approximation of the actual heat fluxes of the film-boiling data. The apparent reduction in heat flux at higher wall temperatures is a result of more heat going into the boiling than into raising the bulk temperature of the fluid.

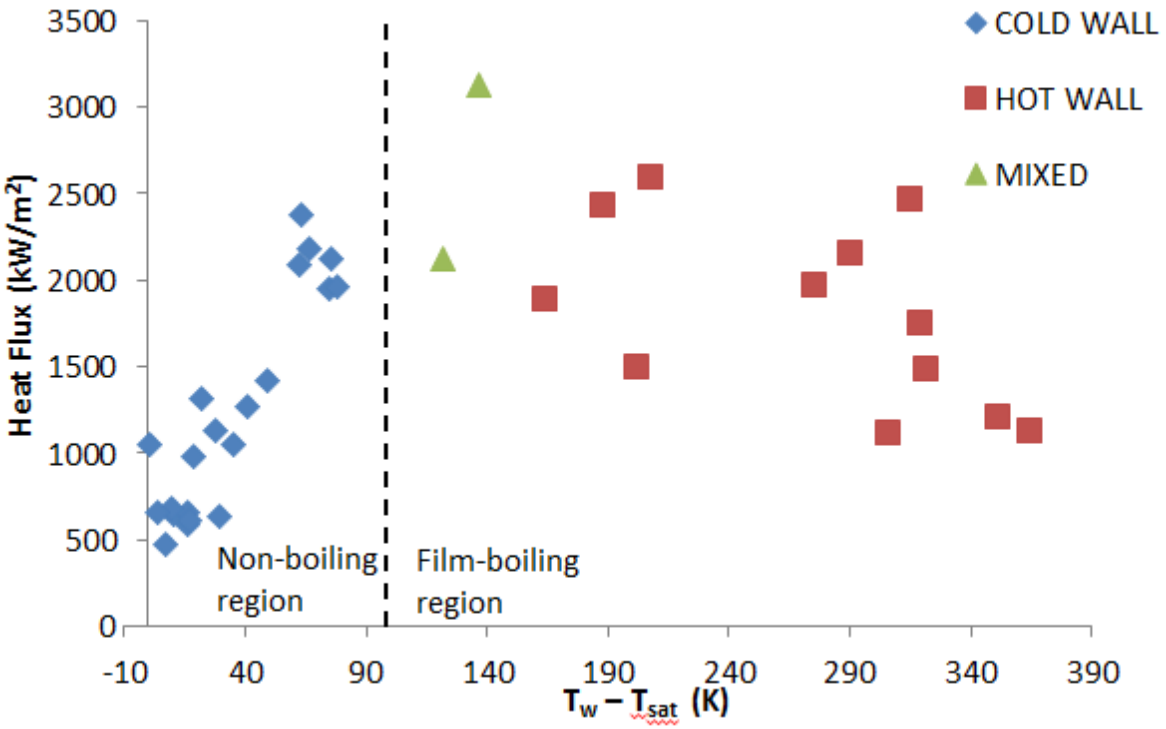


Figure 6.7: Heat Flux as a Function of Average Wall Temperature Minus Saturation Temperature, ($T_w$ – $T_{sat}$), All Velocities Shown, 1.8 mm x 4.1 mm Channel

As shown in Figure 6.7, the measured CHF for the onset of sub-cooled film-boiling is approximately 2,000 kW/m$^2$ at velocities ranging from 7.1 to 14.3 m/s. For comparison, Van Noord reported CHF at approximately 2000 kW/m$^2$ at low velocities (~15 m/s) and up to approximately 5000 kW/m$^2$ at higher velocities [11]. Also, previous studies of methane reported CHF in the 300-1300 kW/m$^2$, scaling with $v^{0.9}$ [12].

It is possible that the "mixed" wall temperature data points capture the transition of the CHF across the temperature rake; the leading three thermocouples read relatively "cool" and the trailing three thermocouples read relatively warm "wall" temperatures. However, since only two data points were achieved in this state, a more conclusive analysis would require more testing.

As noted above, a range of velocities were studied (note all velocities are shown in Figure 6.7). In order to normalize the different data points for the variable velocities, a Boiling Number, *Bo*, was used. The boiling number is defined as the ratio of the critical heat flux, $\dot{q}_{sCHF}$, to the $CH_4$ heat of

vaporization, $i_{fg}$, and mass flow rate per channel cross-sectional area, $A_c$. For this study, all data points were calculated for *Bo* at the measured $\dot{q}_s$ (shown in Eq. (6.8)), in order analyze $\dot{q}_s$ for CHF.

$$Bo = \frac{\dot{q}_s A_c}{i_{fg}\dot{m}} \tag{6.8}$$

Figure 6.8 shows the boiling number, *Bo*, vs. $\Delta T\ (T_w\text{-}T_{sat})$, where $T_{sat}$ refers to the saturation temperature. From this figure, it can be observed that the critical heat flux occurs at a *Bo* value of approximately 0.1.

This value of *Bo* ~0.1 matches well with the Shah correlation for CHF in tube flow, described in Reference [21] In the Shah "upstream conditions correlation", *Bo* is related to a critical length of tube, $z_{crit}$, needed to reach CHF for a given amount of sub-cooling (i.e., negative quality, *x*) in the upstream conditions. Other state properties and geometric parameters are considered in the Shah correlation, but the *Bo* prediction is simplified here for the attention to the primary factors of $(z_{crit}/D_h)$ and $(1\text{-}x)$. In this study, the data points around the measured CHF had sub-cooled quality $x$ ~ -1.3 to -1.4. It is assumed that the CHF occurs before the first wall thermocouple position, which indicates $(z_{crit}/D_h)$ ~2. Based on inspection of the Shah "upstream conditions correlation" plotted in [21], the predicted *Bo* would be ~0.1.

A more complete study of CHF and the validity of the Shah correlation for $LCH_4$ would require more testing in the "mixed" data points, where $z_{crit}$ was more accurately measured across a wide range of mass flow rates and heat fluxes.

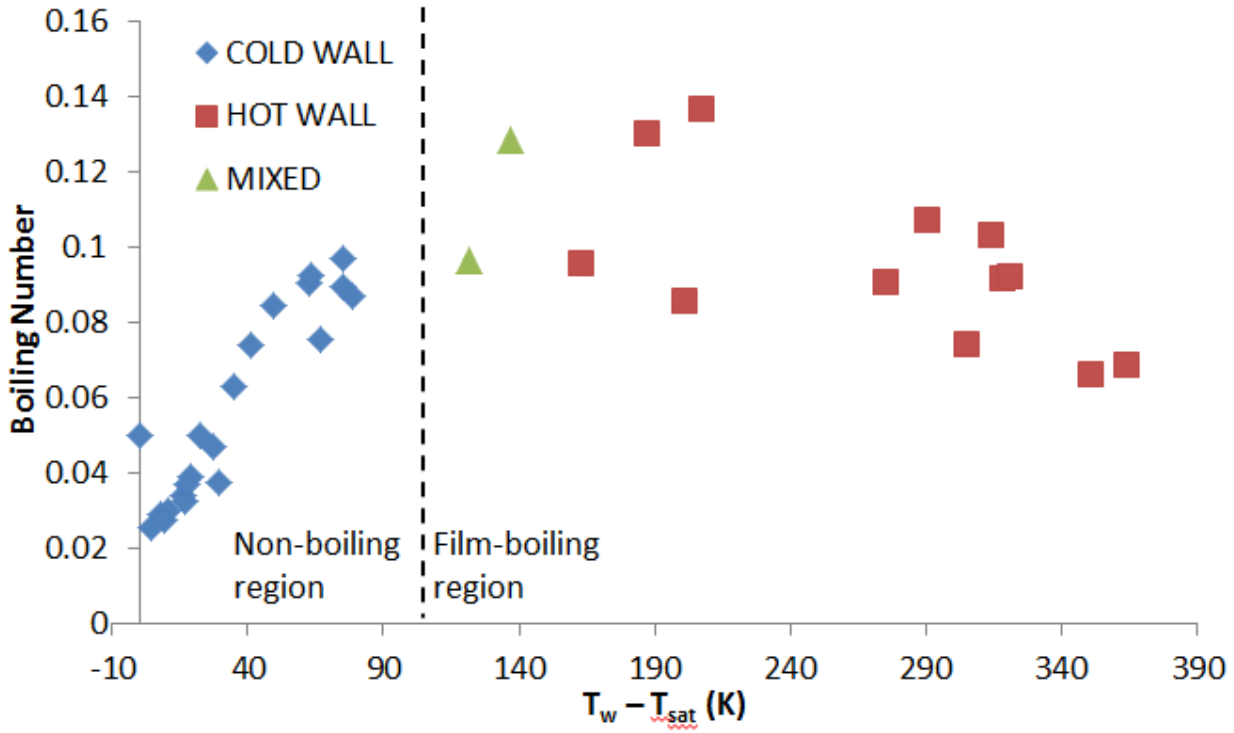


Figure 6.8: Boiling Number as a Function of Average Wall Temperature Minus Saturation Temperature, ($T_w - T_{sat}$), All Velocities Shown, 1.8 mm x 4.1 mm Channel

In 1984, Cook conducted an experimental investigation in which a Nusselt number correlation for supercritical $CH_4$ flowing through smooth channels was developed. Cook's correlation included a temperature correction factor based on a bulk temperature ($T_b$) to wall temperature ($T_w$) ratio [1]. Huzel and Huang also presented a temperature correction factor based on a $T_b$ to $T_w$ ratio which is described for "heat transferred through a vapor film boundary layer" for supercritical propellants [22]. Since heat is being transferred through a vapor film boundary layer in the sub-cooled film-boiling cases, the temperature correction factor was used. Figure 6.9 shows the measured Nusselt number versus the predicted Nusselt number based on Cook's correlation. Recall that the measured Nusselt number only includes the convective component of the heat transfer. Since the temperature correction factor accounts for the heat transferred through a vapor film boundary layer, the film-boiling data lines up well with the non-boiling data [1]. Note that the data scatter in the "cold-wall" single phase test data points is much

broader than the "hot-wall" film-boiling points, and analysis of this data scatter should be considered for future work.

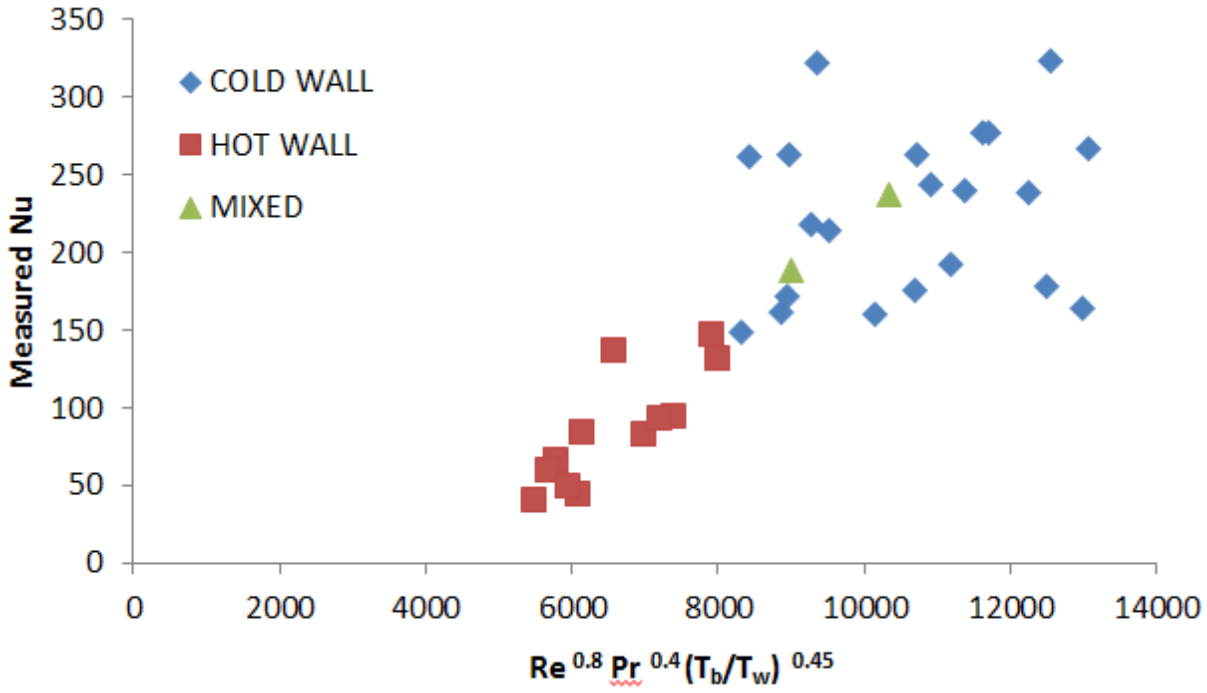


Figure 6.9: Measured Nusselt Number as a Function of Predicted Nusselt Number Based on Cook's Correlation [1], 1.8 mm x 4.1 mm Channel

### 6.3.2 Rough Channels, 3.2 mm x 3.2 mm

The data obtained for the roughened cooling channels includes a total of 24 test points, with six data points per channel; the 24 points include the smooth channel's test points. Similar to the rectangular channel data, boiling phenomena was also present in the rough channel data. Figure 6.10 shows the steady state measured Nusselt number values as a function of the bulk Reynolds number.

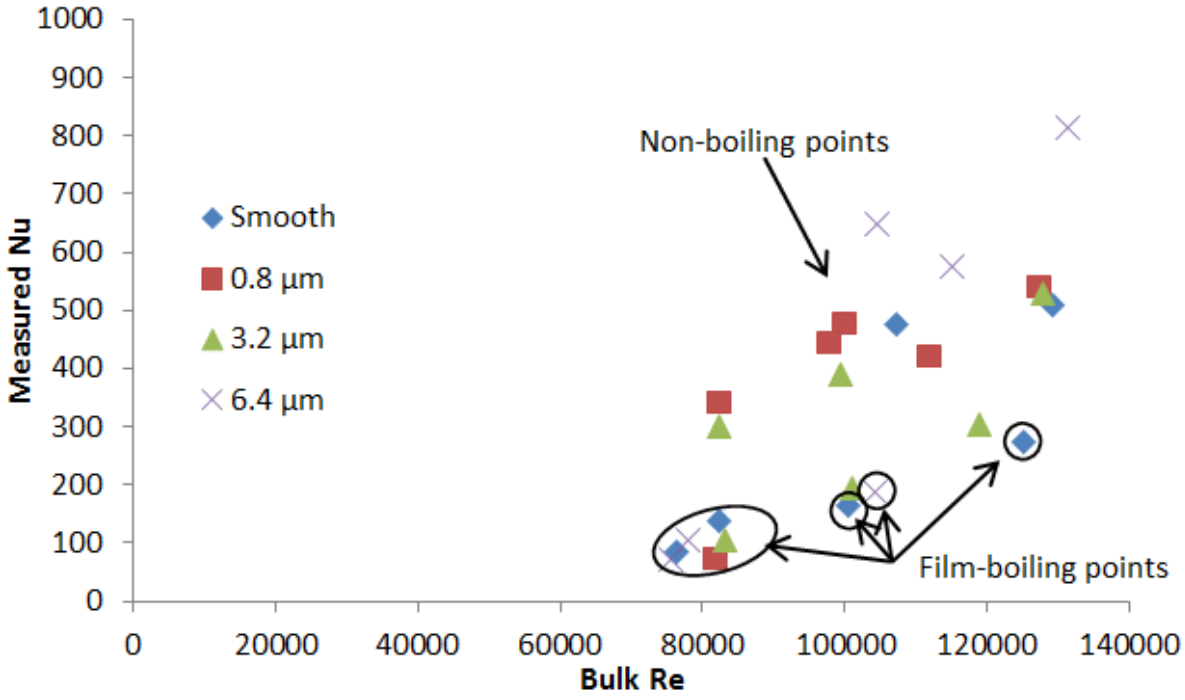


Figure 6.10: Measured Convective Nusselt Number as a Function of Bulk Reynolds Number, 3.2 mm x 3.2 mm Channels

The range of Reynolds numbers obtained for the non-boiling regime is between 82,000 and 131,000, and the Nusselt numbers range between 190 and 810. For the film-boiling regime, Reynolds numbers ranged between 76,000 and 125,000, and Nusselt numbers were between 65 and 270. The same process to distinguish the modes of heat transfer used for the rectangular channel was also used for the roughened channels. The expected trend of increasing heat transfer with increasing surface roughness is not so evident in the single-phase region. That is, the 0.8 and 3.2 µm channels data points overlap with the smooth channel points, whereas only the 6.4 µm channel data points seem to agree with the expected trend of enhanced Nusselt Number. In the film-boiling region, the effects of surface roughness are not distinguishable. To better observe the effects of surface roughness on both heat transfer regimes, more data points should be collected.

Figure 6.11 shows the heat flux values as a function of average wall temperature minus saturation temperature where the different modes of heat transfer can be observed. Figure 6.12 shows the *Bo* vs. $\Delta T$ ($T_w$-$T_{sat}$) plot for the rough channels. The heat flux values were also calculated using the

conservation of energy equation for the steady flow of a fluid in a tube as in Eq. (6.1); therefore, the heat flux values in the film-boiling regime are an approximation and only measure the convective component of the heat transfer. Note that the overall distinction of the CHF for the rough channels is not as obvious as with the smooth rectangular channel study. The overall max *Bo* for CHF was still ~0.1 for the roughened channels, but more testing is required to determine if the roughness has a measurable effect on CHF.

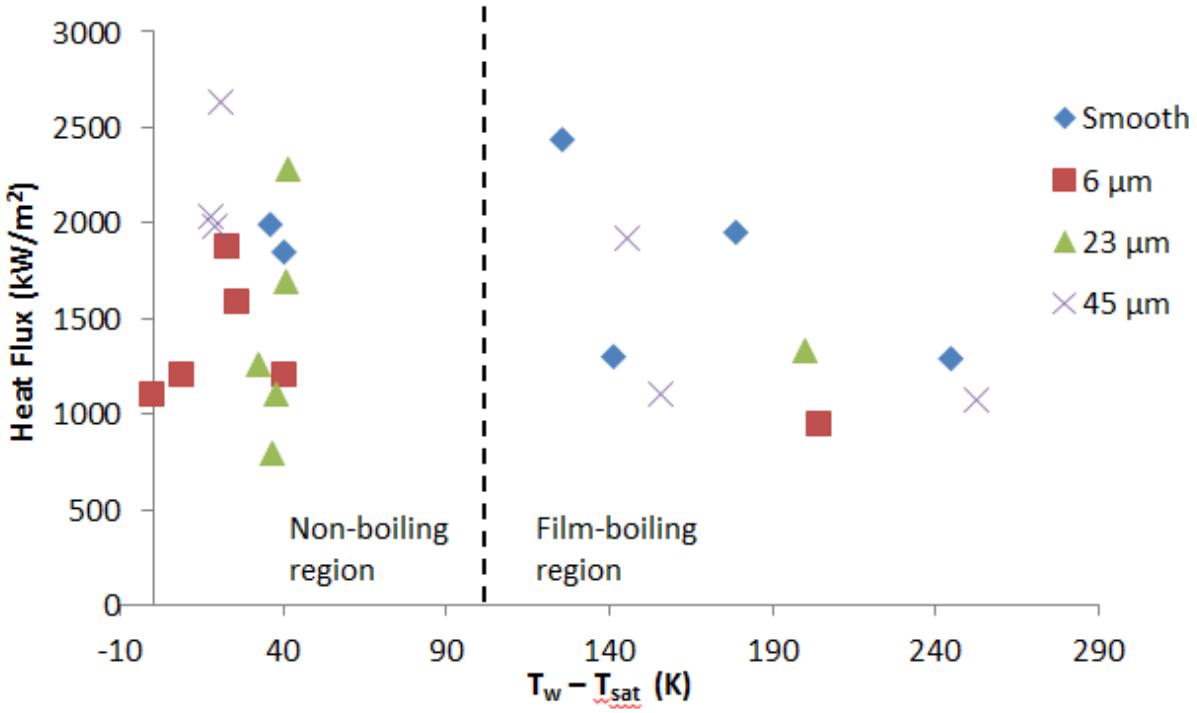


Figure 6.11: Heat Flux as a Function of Average Wall Temperature Minus Saturation Temperature, ($T_w$ – $T_{sat}$), 3.2 mm x 3.2 mm Channels

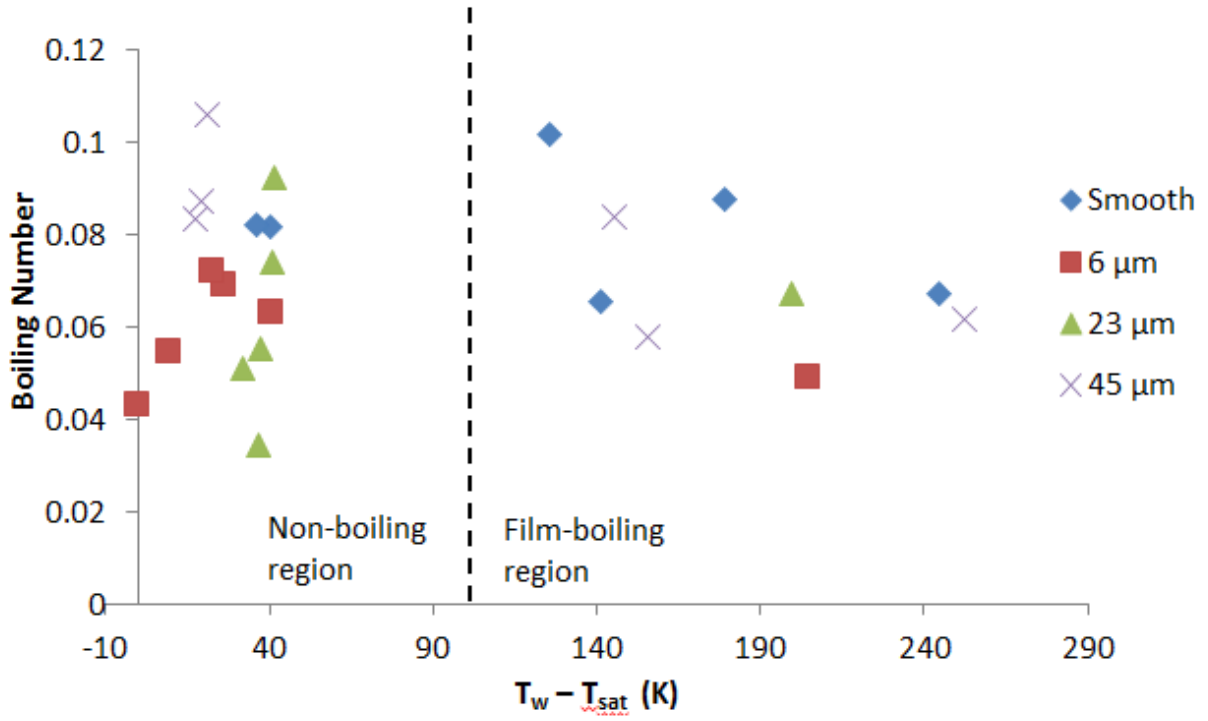


Figure 6.12: Boiling Number as a Function of Average Wall Temperature Minus Saturation Temperature, ($T_w - T_{sat}$), 3.2 mm x 3.2 mm Channels

Similar to the 1.8 mm x 4.1 mm channel, the film-boiling data points lined up with the single-phase range when the $T_b/T_w$ correction factor was used. Since the temperature correction factor accounts for the heat transferred through a vapor film boundary layer, the film-boiling data lines up well with the rest of the points [1]. Figure 6.13 shows the measured Nusselt numbers versus the predicted Nusselt number based on Cook's correlation.

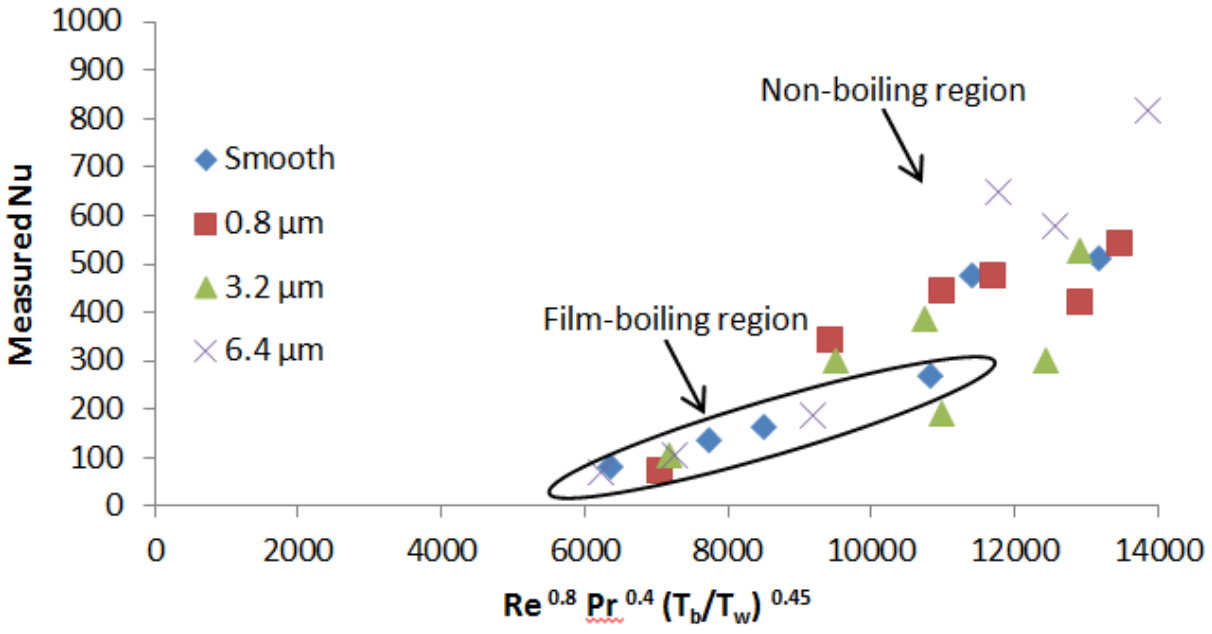


Figure 6.13: Measured Nusselt Number as a Function of Predicted Nusselt Number Based on Cook's Correlation [1], 3.2 mm x 3.2 mm Channels

# Chapter 7: Conclusion

## 7.1 Conclusion

The cooling channels tested serve as a valid representation of cooling channels in a regen engine. Through the use of the HHFTF, a total of 59 steady-state tests were successfully completed to characterize the heat transfer characteristics of $LCH_4$ using five cooling channels. More specifically, the steady state heat transfer characteristics of $LCH_4$ for a channel with a rectangular cross section of 1.8 mm x 4.1 mm were presented. In addition, roughened channels with a square cross section of 3.2 mm x 3.2 mm were also studied. Results stemming from presented experiments are as follows:

Sub-cooled film-boiling phenomena were confirmed in the data pertaining to all the channels presented in this study. For all the channels, the critical heat flux appears to occur at a boiling number value of approximately 0.1. This value matches well with the Shah upstream conditions correlation for CHF in tube flow [21].

A Nusselt number correlation with a temperature correction factor based on a bulk temperature to wall temperature ratio that takes into account the heat transferred to a vapor film boundary layer was used for all channels [1, 22]. The correlation showed to work very well for the film-boiling regime.

For the 1.8 mm x 4.1 mm cooling channel, the measured critical heat flux for the onset of sub-cooled film-boiling is approximately 2000 $kW/m^2$ at velocities ranging from 7.1 to 14.3 m/s which is comparable to the data presented by Van Noord [11].

For the roughened channels, the overall distinction of the CHF is not as obvious as with the smooth rectangular channel study. Also, the effects of surface roughness were not clearly evident in the single phase regime for the channels with roughness values of 0.8 and 3.2 microns. In the film-boiling regime, the heat transfer did not increase with increasing surface roughness, which disagrees with the expected trend.

## 7.2 Future Work

For future work, an analysis to determine the total heat flux in the film-boiling regime should be conducted to fully characterize the heat transfer characteristics of two-phase methane. In addition, an analysis of the data scatter in the single phase regime when applying the Nusselt number correlation

presented in reference [1] should also be performed. For the rough channels, more testing is required to better characterize the effects of surface roughness. More testing is also needed to find the critical heat flux for the range of velocities tested regarding the rough channels.

# References


[1] Cook, R.T. 1984. Methane Heat Transfer Investigation. NASA Marshall Space Flight Center, NASA-CR-171199, Huntsville, AL.

[2] Neill, T. Judd, D. Veith, E. and Rousar, D. 2009. Practical Uses of Liquid Methane in Rocket Engine Applications. Acta Astronautica, Vol. 65, pp. 696-705.

[3] Barry, Patrick. "Methane Blast." NASA Science News. http://science.nasa.gov/science-news/science-at-nasa/2007/04may_methaneblast/

[4] Morehead, R.L. 2011. Project Morpheus Main Engine Development and Preliminary Flight Testing. 47th AIAA Joint Propulsion Conference Atlanta, AIAA 2011-5927, San Diego, CA.

[5] Oberg, E., et al. 2012. Machinery's Handbook. 29th ed. Industrial Press, New York, 2012, p. 739.

[6] Bates, R. W. Mass, E. D. Irvine, S. A. and Auyeung, T. P. 2004. Design of a High Heat Flux Facility for Thermal Stability Testing of Advanced Hydrocarbon Fuels. Air Force Research Laboratory, F04611-99-C-0025, Edwards AFB, CA.

[7] Gage, M.L. Rosenberg, S. D. 1990. Hydrocarbon Fuel/Combustion-Chamber Liner Materials Compatibility. NASA Lewis Research Center, NAS 3-25070, Cleveland, OH.

[8] Irvine S.A., and Burns R.M. 2005. Preliminary Heat Transfer Characteristics of RP-2 Fuel as Tested in the High Heat Flux Facility. Air Force Research Laboratory, AFRL-PR-ED-TP-2005-545, Edwards AFB, CA.

[9] Mass, E. Irvine S.A. Bates, R. and Auyeung T. 2004. A High Heat Flux Facility Design for Testing of Advanced Hydrocarbon Fuel Thermal Stability. Air Force Research Laboratory, 4847, Edwards AFB, CA.

[10] Bates, R.W., Billingsley, M.C., and Lyu, H.Y. 2007. Experimental and Numerical Investigation of RP-2 Under High heat Fluxes. Air Force Research Laboratory, AFRL-PR-ED-TP-2007-150, AFB, CA.

[11] Van Noord, J. 2010. A Heat Transfer Investigation of Liquid and Two-Phase Methane. NASA Glenn Research Center, NASA/TM-2010-216918, Cleveland, OH.

[12] Glickstein, M. R. and Whitesides, R. H. 1967. Forced-Convection Nucleate and Film Boiling of Several Aliphatic Hydrocarbons, ASME-AIChE Heat Transfer Conference and Exhibit, Seattle, WA.

[13] Hongfang, G. Hongzhi, L. Haijun, W. and Yushuan, L. 2013. Experimental Investigation on the Convective Heat Transfer from a Horizontal Miniature Tube to Methane at Supercritical Pressures. Applied Thermal Engineering, Vol. 58, pp. 490-498.

[14] Garcia, C. P. 2013. Pressure and Heat Flux Effects on the Heat Transfer Characteristics of Liquid Methane. PhD Dissertation, University of Texas at El Paso, ProQuest/UMI.

[15] Trejo, A. 2014. An Experimental Investigation of the Cooling Channel Geometry Effects on the Internal Forced Convection of Liquid Methane. PhD Dissertation, University of Texas at El Paso, ProQuest/UMI.

[16] Klimenko, V. V. 1990. A Generalized Correlation for Two-Phase Forced Flow Heat Transfer-Second Assessment. Int. J. of Heat and Mass Transfer, Vol. 33, No. 10, pp. 2073-2088.

[17] Dewan, A. Mahanta, P. Sumithra, K. Suresh P. 2004. Review of Passive Heat Transfer Augmentation Techniques. Proc. Instn Mech. Engrs Vol. 218 Part A: J. Power and Energy

[18] Lemmon, E. W. Huber, M. L. McLinden, M. O. 2013. NIST Standard Reference Database 23: Reference Fluid Thermodynamic and Transport Properties-REFPROP, Version 9.1, National Institute of Standards and Technology, Standard Reference Data Program, Gaithersburg.

[19] Kreith, F., 2000. The CRC Handbook of Thermal Engineering, Boca Raton: CRC Press LLC.

[20] Cengel, Y.A. 2007. Heat and Mass Transfer. 3rd ed., McGraw-Hill, p. 459.

[21] Collier, J. G. and Thome, J. R. 1996. Convective Boiling and Condensation, 3rd edition, Oxford Science Publications, Oxford.

[22] Huzel, D. and Huang, D. 1992. Modern Engineering for Design of Liquid-propellant Rocket Engines, Volume 147, American Institute of Aeronautics and Astronautics, Washington, D.C.

# Appendix

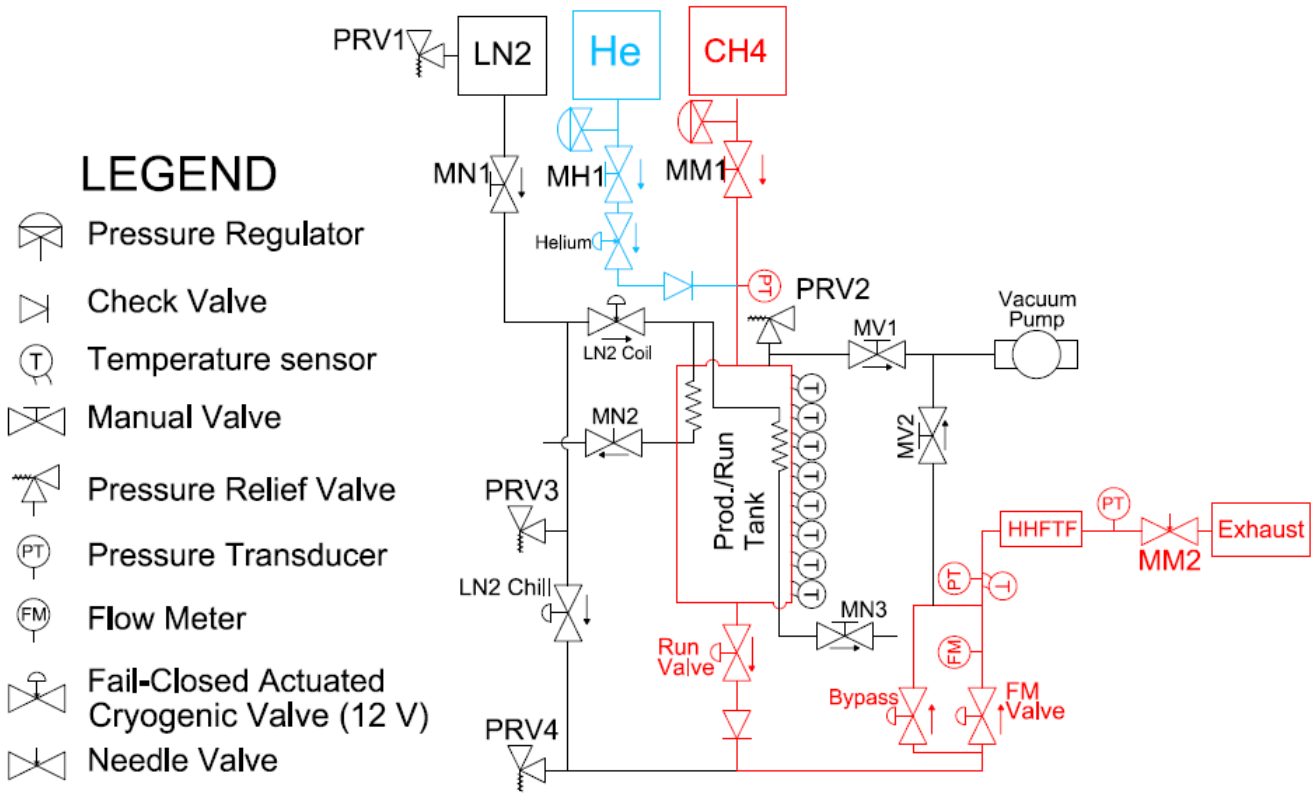


MCU-HHFTF Integrated System Fluid Schematic

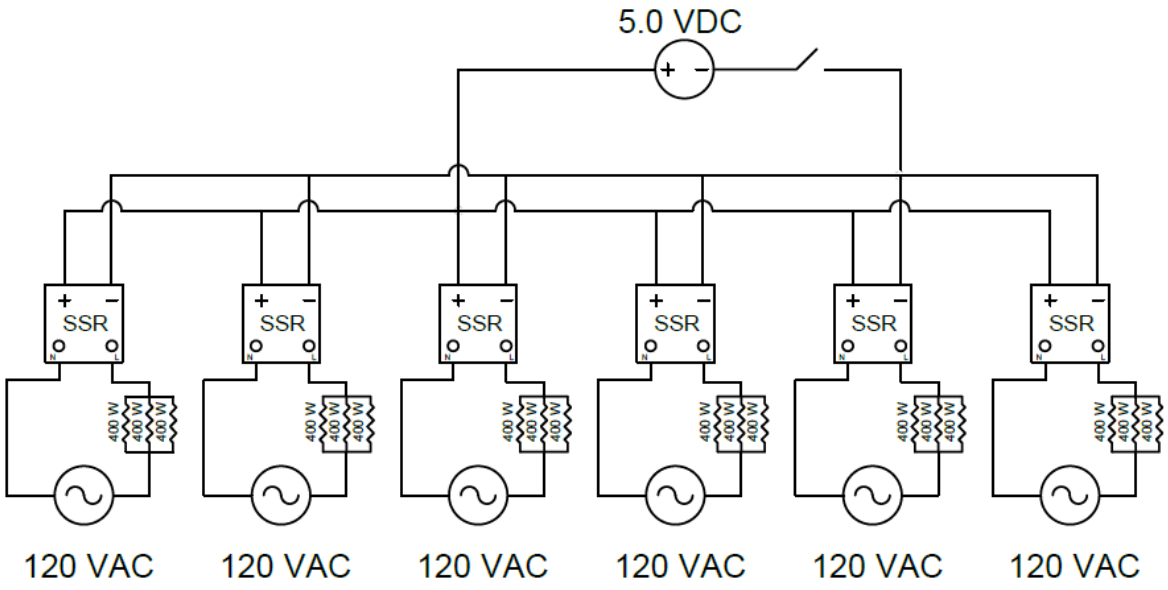


Wiring Schematic of the Cartridge Heater to Solid State Relay Connection

Detailed List of Instrumentation Used in the MCU-HHFTF System

| Item | Make | Model | Range | Accuracy | Use | Quantity |
|---|---|---|---|---|---|---|
| Exposed tip type E thermocouple | Omega Engineering | EMQSS-125E-6 | -200 to 900°C (-328 to 1652°F) | 1.7°C or 0.5% above 0°C, 1.7°C or 1.0% below 0°C | Test section wall temperature measurement | 6 |
| Sheathed ungrounded type E thermocouple | Omega Engineering | EMQSS-125U-6 | -200 to 900°C (-328 to 1652°F) | 1.7°C or 0.5% above 0°C, 1.7°C or 1.0% below 0°C | Test section inlet/outlet and condenser temperature measurement | 8 |
| Nextel ceramic insulated type K thermocouple | Omega Engineering | XC-14-K-12 | -200 to 1250°C (-328 to 2282°F) | 2.2°C or 0.75% above 0°C, 2.2°C or 2.0% below 0°C | Block temperature measurement | 4 |
| Thin Film Cryogenic Pressure Transducer | Omega Engineering | PX1005L-500AV | 0 to 3.45 MPa (0 to 500 psia) -196 to 149°C (-320 to 300°F) | ±0.25% | Condensing/run tank and test section inlet/outlet pressure measurement | 3 |
| Thermocouple Input Module DAQ device | National Instruments | NI 9213 | Refer manual | Refer manual | Thermocouple data acquisition | 2 |
| Terminal Block with SCC Expansion Slots DAQ device | National Instruments | NI SCC-68 | Refer manual | Refer manual | Pressure transducer and flow meter data acquisition | 1 |
| Turbine flow meter DC transmitter | Hoffer Flow Controls, Inc. | CAT315 5DCX1X | -40 to 85°C | ±0.02% of full scale @ 20°C (68°F) | Turbine flow meter data transmission | 1 |
| Pressure transducer process meter and controller | Omega Engineering | DP25B-E-A | 0 to 100 mV | ±0.02% of reading | Pressure transducer signal conditioning | 3 |

| | | | | | | |
|---|---|---|---|---|---|---|
| Convection-enhanced Pirani Sensor | Kurt J Lesker | K31714S | 1 x $10^{-3}$ to 1.0 x $10^{3}$ Torr (1.9 x $10^{-5}$ to 19 psi) | ±<1% | Vacuum chamber pressure measurement | 1 |
| Digital Convection Pirani Vacuum Gauge Controller | MKS | HPS 947 | 1.0 x $10^{-3}$ to 1.0 x $10^{3}$ Torr (1.9 x $10^{-5}$ to 19 psi) | ±<1% | Vacuum chamber pressure digital reading | 1 |

**Detailed Experimental Procedure and Safety Hazard/Risk Mitigation Assessment**
Pre-testing procedure:

1. Inspect instrumentation and equipment.
    a. Turn on power supplies and adjust required voltage.
        i. Actuated valves: 12 VDC.
        ii. Flow meter transmitter: 13-30 VDC.
        iii. SSRs: 5 VDC.
    b. Run the LabVIEW program titled "High Heat Flux Test Facility" located in the "LabVIEW programs" folder in the computer's desktop.
        i. Ensure that LabVIEW program outputs the data file into a folder titled "Methane Test Data" in the computer's desktop.
    c. Ensure that all pressure transducers and thermocouples are reading ambient conditions (13 ± 1 psia and 23 ± 3°C).
    d. Check that all solenoid valves indicated in the schematic function properly by performing an audible and current draw inspection.
        i. Current draw: 1.2 ± 0.1 A.
    e. Connect solid state relays to 120 VAC extension cords.
    f. Using a multi-meter, check that all cartridge heaters work properly by measuring the resistance across them.
        i. Resistance per group of three cartridge heaters is 12 ± 1 ohms.

2. Inspect testing area.
    a. Activate the ventilation system by turning on the ventilation fans.
    b. Check for leaks in the system using snoop liquid leak detector by pressurizing the lines with He to 50 ± 5 psia.
        i. After leak check is performed close He tank valve and vent system
    c. Close needle valve.
    d. Open MV2 valve and pull vacuum in the system with the line vacuum pump.
        i. Line vacuum levels: 2 ± 1 psia.
    e. Activate and configure oxygen monitor and flammable gas detector devices.
        i. Refer to Appendix A for configuration procedures.
    f. Close line vacuum chamber.
    g. Activate the pirani vacuum gauge controller.
    h. Pull vacuum inside the chamber with the chamber vacuum pump.
        i. Chamber vacuum levels: 0.05 ± 0.01 Torr.

3. Prepare for data collection.
    a. Create a folder in the "Methane Test Data" folder that entails the conditions to be tested i.e. heat flux and pressure.

4. Begin methane condensation.
    a. Turn off the line vacuum pump and close MV2 valve.
    b. Open $CH_4$ tank valve.
    c. Open MM1 valve.
    d. Put on cryogenic personal protective equipment (PPE), e.g., gloves, apron, face shield.
    e. Pressurize condensing/run tank to 70 psia.

f. Open MN1 valve and regulate dewar pressure to 150 psig.
g. Open $LN_2$ coil solenoid valve.
h. Open MN2 and MN3 valves.
i. Monitor $LCH_4$ levels using the tank thermocouples.
    i. At 70 psia, methane is liquid at -139°C.
    ii. Tank is filled with $LCH_4$ in 60 ± 15 min.
    **iii. Please note that the condensing process and the block heating process should occur concurrently.**
j. Close $CH_4$ tank valve.

5. Begin heating the copper block.
    a. Manually activate cartridge heaters by following a 3 sec on/off cycle.
        i. Use manual switch located on the switch panel.
    b. Heat the block until desired conditions are reached.
        i. Stop cycling manual switch.
        ii. Refer to test matrix for testing conditions.

Testing procedure:

1. Chill cooling channel and run lines with $LN_2$.
    c. Open $LN_2$ chill and Bypass solenoid valves.
    d. Open needle valve.
    e. Chill until inlet conditions are reached (-160 ± 5°C).
        **i. Please note that chilling and pressurizing run tank occur concurrently.**
    f. Close needle valve.

2. Pressurize run tank with helium.
    a. Open He tank valve.
    b. Open MH1 valve.
    c. Open Helium solenoid valve.
    d. Pressurize run tank to desired conditions.
        i. Refer to test matrix for testing conditions.

3. Stop $LN_2$ flow and adjust needle valve.
    a. Close MN1 valve.
    b. Close $LN_2$ coil and $LN_2$ chill solenoid valves.
    c. Open and adjust needle valve.

4. Begin data recording process.
    a. Flip “Record On” switch to on position on the GUI.

5. Run $LCH_4$ through run lines and cooling channel.
    a. Open Run solenoid valve.
    b. Monitor channel wall and tank temperatures.
        i. Tank temperatures warmer than -150°C indicate depletion of $LCH_4$.
        ii. Observe wall temperature profile in GUI to determine if steady state behavior is reached.
        iii. Channel wall temperature steady state behavior indicates successful test.

c. Close MH1 valve when $LCH_4$ is depleted.
d. Close Run solenoid valve and needle valve.

6. Stop data recording process.
    a. Flip "Record On" switch to off position on the GUI.

Post-testing procedure:

1. Close He tank valve.

2. Relieve residual system pressure.
    a. Open run solenoid valve.
    b. Gradually open needle valve.
    c. Check that all manual and solenoid valves are open to prevent pressure build up from residual fluids.
    d. Monitor system until ambient conditions are reached.

3. Deactivate all electronic devices.
    a. Turn off chamber vacuum pump.
    b. Check cartridge heaters' resistance to test functionality.
    c. Disconnect solid state relays from 120 VAC extension cords.
    d. Turn off power supplies.
    e. Turn off oxygen meter and flammable gas detector devices.

4. Check that data was collected and transfer it for processing.
    a. Data is used to find the heat transfer coefficient of methane and derive Nusselt number correlations.

**Emergency Procedure**

All safety considerations were taken and an emergency procedure was developed in case of an unwanted occurrence. Red lines are shown below to avoid a catastrophic failure of the hardware or facilities.

Red Lines:

- Line pressure must remain less than 350 psia.
- Methane tank pressure must remain less than 500 psia.
- Block temperature must remain less than 500°C.

Risks and Hazards:

| Hazard | Risk | Mitigation |
|---|---|---|
| Cryogenics | Cold contact burns, explosion (pressure), asphyxiation | Cryogenic PPE, pressure relief valves, oxygen monitor device |
| Flammability | Burns, explosion (ignition) | Fire extinguisher, dilution of $LCH_4$ |

# Vita

Abraham Gerardo Trujillo was born in El Paso, Texas and raised in Ciudad Juarez, Mexico. He attended the University of Texas at El Paso starting the fall of 2005 and graduated with a Bachelor's of Science degree in Mechanical Engineering in the spring of 2010. He started working at the Center for Space Exploration Technology Research in spring of 2012 while pursuing a Master's of Science degree in Mechanical Engineering. In the summer of 2013, he interned at NASA Johnson Space Center and worked on the development of a partial regeneratively-cooled lander class engine. His research focus is propulsion technologies, specifically LOX/Methane regeneratively-cooled engines.

Permanent address: 712 Oscar Perez Ave
El Paso, TX, 79932

This thesis was typed by Abraham Gerardo Trujillo.